



HAL
open science

Light in the Cave: Opal coating detection by UV-light illumination and fluorescence in a rock art context. Methodological development and application in Points Cave (Gard, France)

Marine Quiers, Claire Chanteraud, Andréa Maris-Froelich, Emilie Chalmin, Stéphane Jaillet, Camille Noûs, Sébastien Pairis, Yves Perrette, Hélène Salomon, Julien Monney

► **To cite this version:**

Marine Quiers, Claire Chanteraud, Andréa Maris-Froelich, Emilie Chalmin, Stéphane Jaillet, et al.. Light in the Cave: Opal coating detection by UV-light illumination and fluorescence in a rock art context. Methodological development and application in Points Cave (Gard, France). 2022. hal-03383193v3

HAL Id: hal-03383193

<https://hal.science/hal-03383193v3>

Preprint submitted on 7 Mar 2022 (v3), last revised 14 Jun 2022 (v5)

HAL is a multi-disciplinary open access archive for the deposit and dissemination of scientific research documents, whether they are published or not. The documents may come from teaching and research institutions in France or abroad, or from public or private research centers.

L'archive ouverte pluridisciplinaire **HAL**, est destinée au dépôt et à la diffusion de documents scientifiques de niveau recherche, publiés ou non, émanant des établissements d'enseignement et de recherche français ou étrangers, des laboratoires publics ou privés.

Light in the Cave: Opal coating detection by UV-light illumination and fluorescence in a rock art context

Methodological development and application in Points Cave (Gard, France)

Marine Quiers ^{a*}, Claire Chanteraud ^{b,c}, Andréa Maris-Froelich ^a, Émilie Chalmin-Aljanabi ^c, Stéphane Jaillot ^c, Camille Noûs ^e, Sébastien Pairis ^d, Yves Perrette ^{c,b}, Hélène Salomon ^c, Julien Monney ^c

^aLaboratoire Commun SpecSolE, Envisol – CNRS - Univ. Savoie Mont Blanc, Chambéry, 73000, France

^bMissouri University Research reactor - University of Missouri 65203 Columbia MO

^cEDYTEM UMR5204, CNRS, Univ. Savoie Mont Blanc, Chambéry, 73000, France

^dUniv. Grenoble Alpes, CNRS, Grenoble INP, Institut Néel, Grenoble, 38000, France

^eLaboratoire Cogitamus, 1 ¾ rue Descartes, Paris, 75005, France

* Corresponding author: m.quiers@envisol.fr

Abstract

Silica coatings developed on rock art walls in Points Cave question the access to pictorial matter specificities (geochemistry and petrography) and the rock art conservation state in the context of pigment studies. However, classical *in situ* spectroscopic techniques appear unsuccessful to identify these coatings, which also prevent pigment characterization. In this study, we propose using a UV fluorescence method for opal coating detection based on the fluorescence specificities of uranyl-silica complexes composing these deposits. A coupling of spectral identification using UV laser-induced fluorescence spectroscopy with UV illumination was performed on samples and μ -samples from the Points Cave rock art site. The well-defined peaks observed in fluorescence emission spectra due to uranyl ions validate opal detection and its correspondence with green fluorescence observed under UV light at micro- and macroscopic scales. *In situ* optical measurements under UV illumination reveal the presence of opal coating, especially on rock art walls in Points Cave. Opal occurrence and repartition observations provide the first insights into Points Cave wall evolution and chronological constraints linked to opal coating development. Regarding the strong interactions with pigment suggested by

35 multiscale observations of samples and μ -samples, the impact of the presence of opal coating on
36 Points Cave rock art conservation quality is questioned. Thus, by developing a specific and non-
37 destructive characterization method for opal coatings, this study opens up a new approach for the
38 study of decorated wall taphonomy and proposes utilizing mineralization both as markers of the
39 natural history of caves and as an indication for their occupation by ancient human groups.

40

41 **Keywords:** Silica coating, uranyl, UV fluorescence, *in situ* detection, rock art cave, Quaternary,
42 archaeology, Ardèche, France, optical methods

43

44

45 **1. Introduction**

46 Natural activity in caves, mostly water weathering (Delvigne, 1998; Chalmin *et al.*, 2019; Salomon *et*
47 *al.*, 2021), transforms by physical, chemical, biological and mechanical action the surface of the walls.
48 Thus, the traces of all these transformations (environmental input) can be a source of information
49 regarding natural and anthropological events on the wall surface, such as drawing and painting
50 realizations, cave environment evolution, and human attendance in the cave (Sadier, 2013; Pons-
51 Branchu *et al.*, 2014; Quilès *et al.*, 2015; Shao *et al.*, 2017; Valladas *et al.*, 2017; Money & Jaillet,
52 2019).

53

54 Among the taphonomic processes impacting rock art pictorial matter, mineral-coating formation as
55 weathering products is well described in rock art research (Vignaud *et al.*, 2006; Huntley, 2012;
56 Bassel, 2017; Chalmin *et al.*, 2018; Mauran *et al.*, 2019). Silica rich amorphous deposits, also called
57 silica skins, have been observed at different cave and open-air parietal sites (Watchman, 1990; Aubert
58 *et al.*, 2004; Aubert *et al.*, 2012; Huntley, 2012). Studies have suggested both a positive and negative
59 impact on rock art conservation due to opal coating development. Indeed, the strong interaction
60 suspected with hematite pigments has been suggested as an element of conservation enhancement,

61 notably compared with other pigments (Watchman, 1990). However, some authors have also observed
62 exfoliation processes of silica skins, which could play a role in rock art weathering (Aubert *et al.*,
63 2004; Green *et al.*, 2017). To our knowledge, there is still no clear answer on the role of silica coatings
64 as conservation factors of pictorial matter. In addition to this conservation issue, silica skins have been
65 proposed as tools for indirect dating of parietal art, especially in the case of inorganic pictorial matter
66 (Aubert *et al.*, 2004; Aubert *et al.*, 2012). Indeed, this mineral phase is known to be enriched in uranyl
67 ions, but the U-Th dating application remains hypothetical due to silica skin thickness and absence of
68 stratigraphy, which complicate both sampling and measurement reliability (Green *et al.*, 2017).

69

70 Thus, silica skin characterization represents a key issue in the rock art context, however it remains
71 difficult to identify and characterize, especially with non-invasive techniques. Currently, the use of *in*
72 *situ* spectroscopic techniques in rock art studies is increasing, as these methods can provide
73 information on both pictorial matter and pigment environments (substrate, deposits, concretions, etc.).
74 The portability and decreasing cost of instruments coupled with the rapidity and the non-destructive
75 character of analyses have led to a quasi-systematic use of these techniques in recent rock art studies
76 (Huntley, 2012, Mauran *et al.*, 2019; Trosseau *et al.*, 2021; Chanteraud *et al.*, 2021). However,
77 amorphous silica characterization, even in the rock art context, is generally based on laboratory
78 observations such as SEM or XRD analyses (Watchman, 1990; Gaillou *et al.*, 2008; Garcia-Guinea *et*
79 *al.*, 2013; Huntley *et al.*, 2015; Green *et al.*, 2017). In addition, the signal of pictorial matter acquired
80 with portable spectroscopic techniques could be impacted by the presence of silica skins, as observed
81 by Huntley (2012) in the case of pXRF measurements.

82

83 In this paper, we propose a new method for the *in situ* detection and characterization of amorphous
84 silica in a rock art context based on UV laser-induced fluorescence (LIF). Indeed, uranyl fluorescence
85 characteristics under UV light are well known and have been observed in silica mineralization,
86 especially in opal (deNeufville *et al.*, 1981; Gorobets *et al.*, 1977; Fritsch *et al.*, 2001; Gaillou *et al.*,
87 2008). Thus, UV spectroscopy presents the same advantages as other portable spectroscopic

88 techniques, but the bright green fluorescence and the specific spectral features displayed by uranyl
89 ions enable the targeted identification of opal coatings. To our knowledge, only one study has reported
90 opal detection in caves using optical methods based on UV techniques (Garcia-Guinea *et al.*, 2013),
91 and no study has applied UV spectroscopic methods in a rock art context for opal identification. Here,
92 we propose a methodological development based on laboratory and field experiments to validate the
93 use of *in situ* UV techniques for opal detection in a rock art context by coupling *in situ* optical and
94 spectroscopic analyses to obtain multiscale information.

95

96 This study was performed in Points Cave (Aiguèze, Gard, France), which contains an important spread
97 of opal coating on the cave walls. In this approach, Points Cave perfectly illustrates the importance of
98 environmental input characterization in the study of rock art (Chanteraud *et al.*, 2021). The advantage
99 of this site is given by the presence of colouring flakes falling from cave walls, allowing transport, μ -
100 sampling and analysis in the laboratory. Analysis of these coloured flakes allows us to identify and
101 measure the environmental input, which modifies and obscures the identification of pictorial matter
102 characteristics.

103

104 **2. Material**

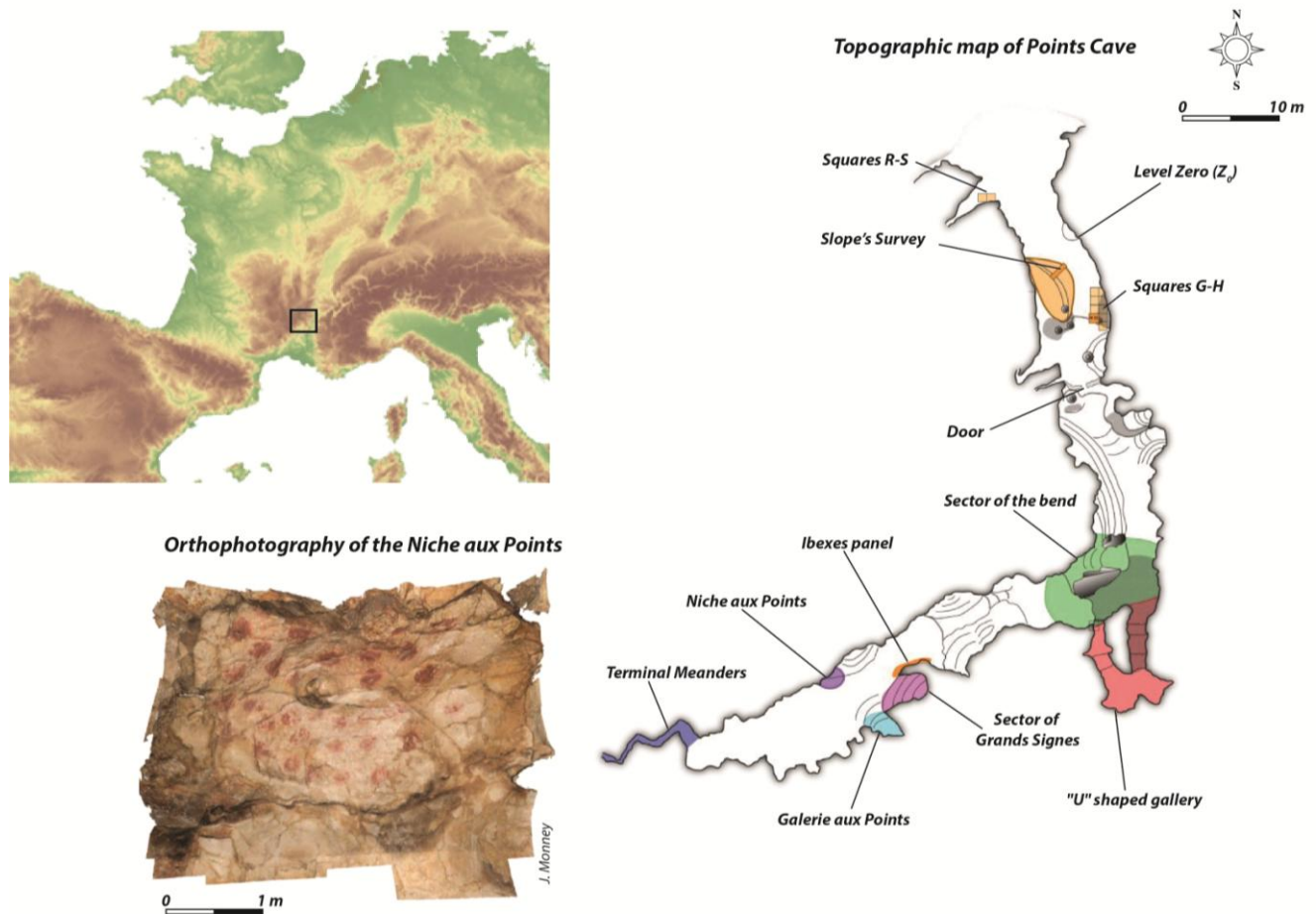
105

106 **2.1 Study site: Points Cave**

107

108 Located in the Ardèche River Canyon, less than 10 km downstream of Chauvet Cave, Points Cave is a
109 Palaeolithic rock art site identified in 1993 (Figure 1) (Deschamps *et al.*, 2018). Archaeological studies
110 have been performed since 2011 as part of the “Datation Grottes Ornées” project (“Cave Art Dating”
111 project, Monney, 2011; 2018). The entrance opens on a hundred-metre long gallery in Urgonian
112 limestone. The rock art which is exclusively composed of red drawings and paintings, is located in the
113 middle part of the gallery preserved from sunlight. Excavations conducted at the entrance indicated
114 human and animal occupation during the Upper Palaeolithic (Figure 1) (Monney & Jaillet, 2019).

115



116

Figure 1: Points Cave location in southeastern France, topographic map of the cave with location of the excavations and the rock art panels (J. Monney); orthophotography of the “Niche aux Points” panel (S. Jaillet)

117

118 Points Cave is currently disconnected from hydrogeological flows (Jaillet & Monney, 2018). Only a
119 few infiltrations can be observed after strong precipitation events. The low level of leaching on the
120 wall and the quasi-absence of a calcite veil are due to this weak hydrogeological activity. Millimetric
121 to centimetric concretions and efflorescence’s (coralloid type of crystallization) have also developed
122 on the wall surface in the decorated sector (Mauran, 2019 in Monney et al., 2019; Barbaran & Nouet,
123 2020).

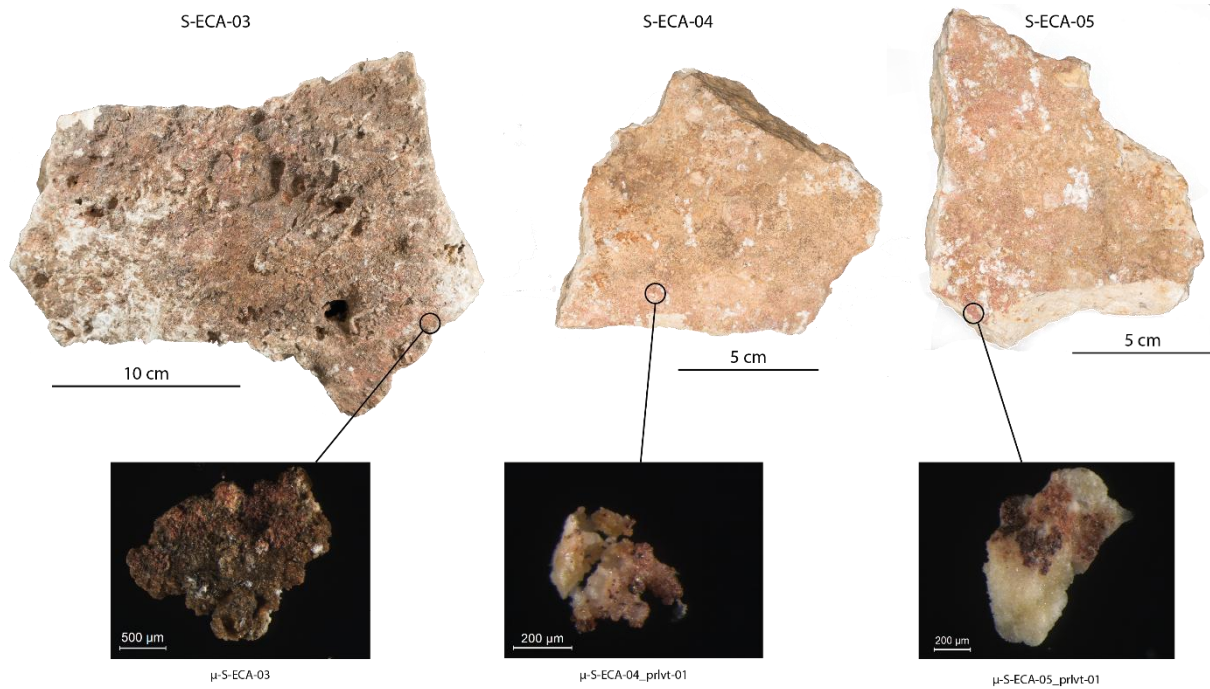
2.2 Points Cave pictorial matter

124
125
126
127
128
129
130
131
132
133
134
135
136
137
138
139
140
141
142
143
144
145
146
147
148
149
150

Parietal ornamentation, composed exclusively of reddish tracings and paintings, is currently observed in the middle part of the gallery. It comprises 59 palm-printed dots, commonly referred to as "palm points". This ornamentation also consists of five animal representations (three ibexes, a horse and a bison), two bilobed signs, an angular line and a few indeterminate traces (isolated lines and dots) (Monney, 2018). Moreover, archaeological colouring matter has been found in the sedimentary sequence at the entrance of the cave (Chanteraud *et al.*, 2019; Chanteraud, 2020).

Investigations carried out at the foot of the rock art panel known as the "Great Signs" found five coloured wall flakes on the ground in the chaos of rocks: S-ECA-01 to S-ECA-05. These 3 to 20 cm flakes are composed of limestone detached from the wall by mechanical action and covered on one side with colouring matter (Monney, 2011). The flakes come more than likely from the large bilobed sign (graphic entity PTS-10) or from other unknown rock art panels that may have crumbled entirely from the walls nearby (Monney, 2018). These flakes are a major asset of Points Cave because they allowed to access the cave walls surface with accurate instruments by bringing the fragment of rock art (flakes) in the laboratory.

To identify both the iron-oxide morphologies and the natural mineralization that can form on the surface of the decorated walls, our study was focused on three of the five wall flakes (S-ECA-03, S-ECA-04, S-ECA-05) discovered in the decorated sector of Points Cave, because of the presence of opal coating on their surface (Figure 2). μ -sampling of pictorial matter was performed on the coloured flakes: μ -S-ECA-03, μ -S-ECA-04, μ -S-ECA-05. These last two have been fragmented during sampling giving: μ -S-ECA-04_prlvt_01, μ -S-ECA-04_prlvt_02 and μ -S-ECA-04_prlvt_03, and μ -S-ECA-05_prlvt_01 and μ -S-ECA-05_prlvt_02 (S.I.1).



151

152 **Figure 2:** Limestone flakes found at the foot of the Bilobed Signs panel and location of μ -sampling.

153

154 To illustrate the rock art surfaces in the cave, 12 μ -samples of pictorial matter on limestone and 8 μ -
 155 samples from the naked wall (limestone) taken from the decorated panels of the cave, were added to
 156 the study (Table 1, S.I.2). All μ -samples of pictorial matter were observed and analysed without any
 157 preparation.

158

159 **Table 1:** Inventory of μ -samples with colouring matter coming from the rock art panels

160

<i>Sample N°</i>	<i>Graphic entities</i>	<i>Type</i>
– Ibexes Panel –		
<i>Prm-19-01</i>	<i>Near to the Ibex n°5</i>	<i>Wall Blank</i>
<i>Prm-19-02</i>	<i>Ibex n°5</i>	<i>Pictorial matter</i>
– Horse Panel –		
<i>Prm-19-03</i>	<i>Near to the Horse</i>	<i>Wall Blank</i>
<i>Prm-19-04</i>	<i>Horse n°7</i>	<i>Pictorial matter</i>
<i>Prm-19-05</i>	<i>Bison n°8</i>	<i>Pictorial matter</i>
– Great Signs Panel –		
<i>Prm-19-06</i>	<i>Near to the Sign n°9</i>	<i>Wall Blank</i>

Prm-19-07	Small Bilobe Sign n°9	Pictorial matter
Prm-19-08	Great Bilobe Sign n°10	Pictorial matter
Prm-19-09	Palm-Dot n°14-02	Pictorial matter
Prm-19-10	Angular Sign n°13	Pictorial matter
– Dots Galerie –		
<i>Prm-19-11</i>	<i>Near to the Palm-Dot n°11-02</i>	<i>Wall Blank</i>
Prm-19-12	Palm-Dot n°11-02	Pictorial matter
Prm-19-13	Palm-Dot n°11-03	Pictorial matter
– Dots Galerie (assamblage 11) –		
<i>Prm-19-14</i>	<i>Near to the Palm-Dot n°11-01</i>	<i>Wall Blank</i>
Prm-19-15	Palm-Dot n°11-01	Pictorial matter
Prm-19-16	Palm-paume n°15-21	Pictorial matter
Prm-19-17	Palm-paume n°15-01	Pictorial matter
– Niche aux Points –		
<i>Prm-19-18</i>	<i>In the center of the panel</i>	<i>Wall Blank</i>
– Entre Secteur des Bouquetins et du Cheval –		
<i>Prm-19-19</i>	<i>On the limestone</i>	<i>Wall Blank</i>
– Niche aux Points –		
<i>Prm-19-20</i>	<i>Near to the Palm-Dot</i>	<i>Wall Blank</i>

161

162

163 3. Methods

164

165 3.1 Macroscopic and microscopic observations

166

167 3.1.1 Laboratory and in situ observations at macroscopic scale

168

169 Image capture for macroscopic observations was performed in two steps: 1) a photograph was taken
 170 under white light, and 2) another photograph was taken under UV light illumination. Observations at
 171 the macroscopic scale in the laboratory and in the cave were realized with a Canon EOS 5D Mark III
 172 camera and a Canon EOS 7D camera fixed on a tripod. A detached flash was used for image capture
 173 under white light. For UV light illumination, 4 UV LEDs (280 nm, 2.26 W, NewEnergy) were fixed
 174 on orientable macroflash bars on each side (2 LEDs per side) of the camera, allowing both
 175 macrophotography and general views of cave walls. Camera parameters are available in Table 2.

Table 2: Camera parameters used for both white and UV light illumination during field and laboratory macroscopic observations.

			<i>Aperture</i>	<i>Obturation speed (sec)</i>	<i>Iso</i>
Laboratory	White light		F/7.1	1/320	1600
	UV light		F/7.1	10	1600
Field	White light	<i>Macro</i>	F/11	½	320
		<i>Wall view</i>	F/11	1/60	100
	UV light	<i>Macro</i>	F/4.5	½	320
		<i>Wall view</i>	F/11	15	320

177

178 Laboratory observations were also performed using a stereomicroscope (LEICA M165 C) under white
179 and UV light. The same 4 LEDs were used for UV illumination.

180

181 3.1.2 Laboratory observations at the microscopic scale

182

183 At the microscopic scale, observations of μ -samples of flakes on carbon tape were realized with a
184 field-emission scanning electronic microscope (SEM) ZEISS Ultra+ associated with an EDX (energy
185 dispersive X-ray) probe (SDD, Bruker) working in high-vacuum mode with a 15 keV voltage. Images
186 were taken with secondary electrons using in-lens or Everhart-Thornley detectors (SE2) and with
187 backscatter electrons (BSE-AsB detector) (Néel Institut, Grenoble).

188

189 3.2 UV fluorescence analyses

190

191 Stationary fluorescence signal of flake and flake μ -samples was measured in the laboratory with a

192 solid-phase spectrofluorimeter designed in the EDYTEM laboratory for non-destructive solid-phase
193 measurements (Perrette *et al.*, 2000).

194
195 This instrument is divided into excitation and detection compartments associated with a translation
196 stage system for sample surface measurement. For this experiment, the excitation system was
197 composed of a Nd:YAG laser (Crylas, FQSS266-Q1) with a 266 nm excitation wavelength. The
198 fluorescence emission response was collected after sample excitation by focusing the laser beam (~30
199 μm) on its surface. The detection system was composed of a low-pass filter monochromator (Jobin
200 Yvon, MicroHr) for light diffraction, fitted with a 300-g/mm diffraction-grating centred at 620 nm,
201 associated with a thermoelectric-cooled, back-illuminated CCD (Jobin Yvon, Sincerity) for high-
202 efficiency signal detection in the UV-visible light domain. As no manipulation, modification or
203 destruction of the sample surface occurred during analysis, this technique is suitable for archaeological
204 sample measurements.

205
206 Two types of fluorescence measurements were realized:

- 207 - Single point measurements were performed on flake μ -samples (μ -S-ECA-03, μ -S-ECA-04
208 and μ -S-ECA-05-02, S.I.3). One spectrum was independently acquired on the sample.
209 Measurement location was determined manually. An acquisition time of 1 s and a
210 monochromator entrance slit of 0.25 mm (~1 nm spectral resolution) were used for spot
211 spectrum acquisition.
- 212 - Surface measurement was performed on flake S-ECA-05 (S.I.4). The motorized translation
213 stage system allowed movements in two directions for surface measurements. The image was
214 obtained by stacking lines along the Y-axis. For this study, fluorescence surface imaging was
215 performed with a 100 \times 100 μm resolution using a 0.1 s acquisition time and a 0.05 mm
216 entrance slit.

217
218 Data pre-processing was performed with MATLAB software (S.I.5). Spectra were corrected from

219 baseline and instrument responses and then filtered with the Savitsky-Golay method (Savitzky &
220 Golay, 1964).

221

222

223 **4. Results**

224

225 *4.1 Macroscopic scale observations*

226

227 At the macroscopic scale (by visual inspection), beside the centimetric coralloid crystallization there is
228 no other mineralization visible than the limestone on the walls, flakes or μ -sample surfaces. In fact, at
229 this observation scale, surfaces seemed to be well preserved with strong colouration from the pictorial
230 matter and clear access to the calcareous substrate (Figure 2).

231

232 Despite the results of the visual inspection of the walls and the observation of the μ -samples both of
233 the rock art and the flakes under stereomicroscope, pXRF analyses (1cm^3 spot) showed that decorated
234 panels of the cave display mineralizations, such as calcium sulphate (Chanteraud *et al.*, 2020; S.I.6).
235 This contradiction between observation and geochemical analysis reveals the need for microscopic
236 inspection using SEM device.

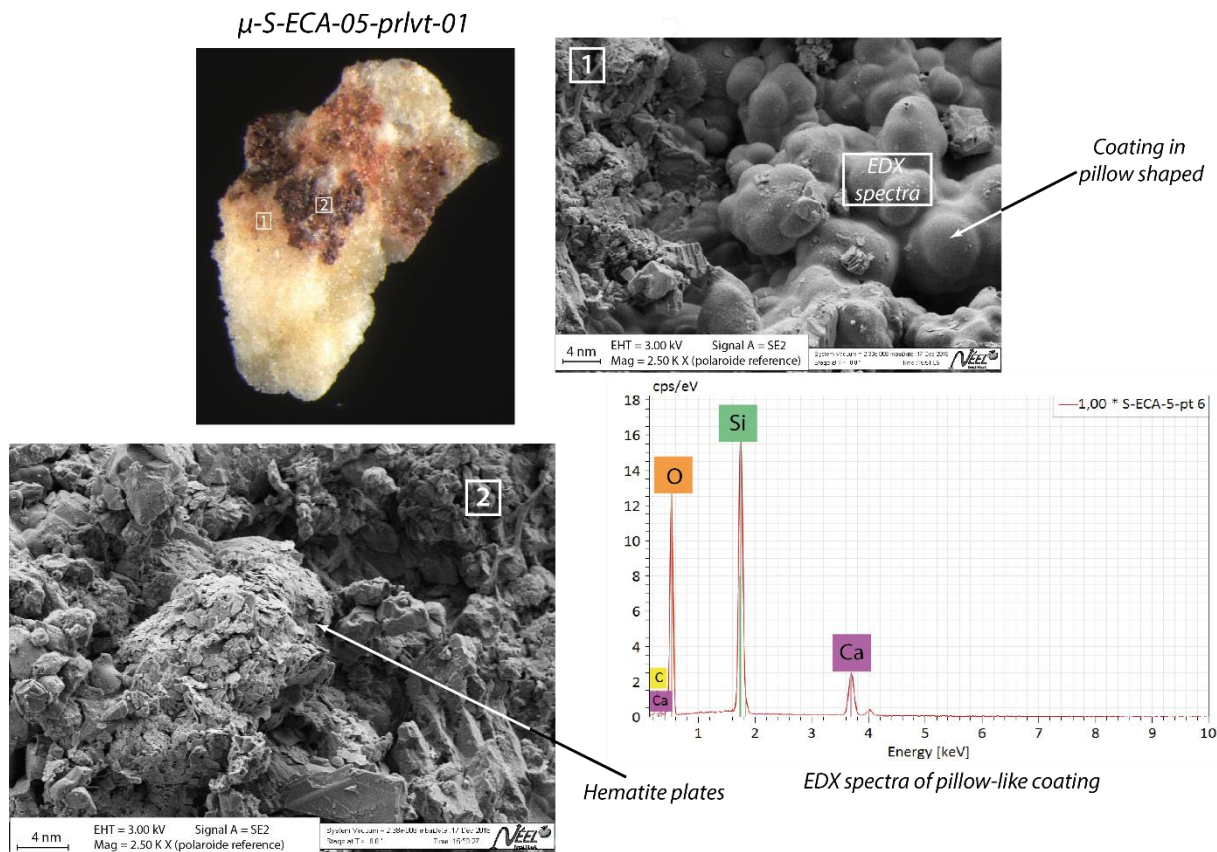
237

238 *4.2 Microscopic scale observations*

239

240 At the microscopic scale, a $1\ \mu\text{m}$ -thin mineral film consisting of nonordered spheres was identified as
241 silica mineralization on μ -S-ECA-03, μ -S-ECA-04-prlvt-02, μ -S-ECA-05-prlvt-01 (Figure 3; S.I.2).
242 However, μ -S-ECA-03 shows less opal coating than the two other μ -samples. The geochemistry and
243 hummocky morphology of the opal could be related to a type A-g amorphous opal with a $\text{SiO}_2 \cdot n\text{H}_2\text{O}$
244 formula (Flörke *et al.*, 1991). The mineral structure present on coloured flakes suggested its formation
245 from a water film containing a high concentration of silica (Monger & Kelly, 2002; Curtis *et al.*,

246 2019). With this mode of formation, it is difficult to assume if the opal came before the hematite
 247 deposit. In fact, it is possible that the opal coating grows at the interface between the limestone
 248 substrate and the colouring matter.



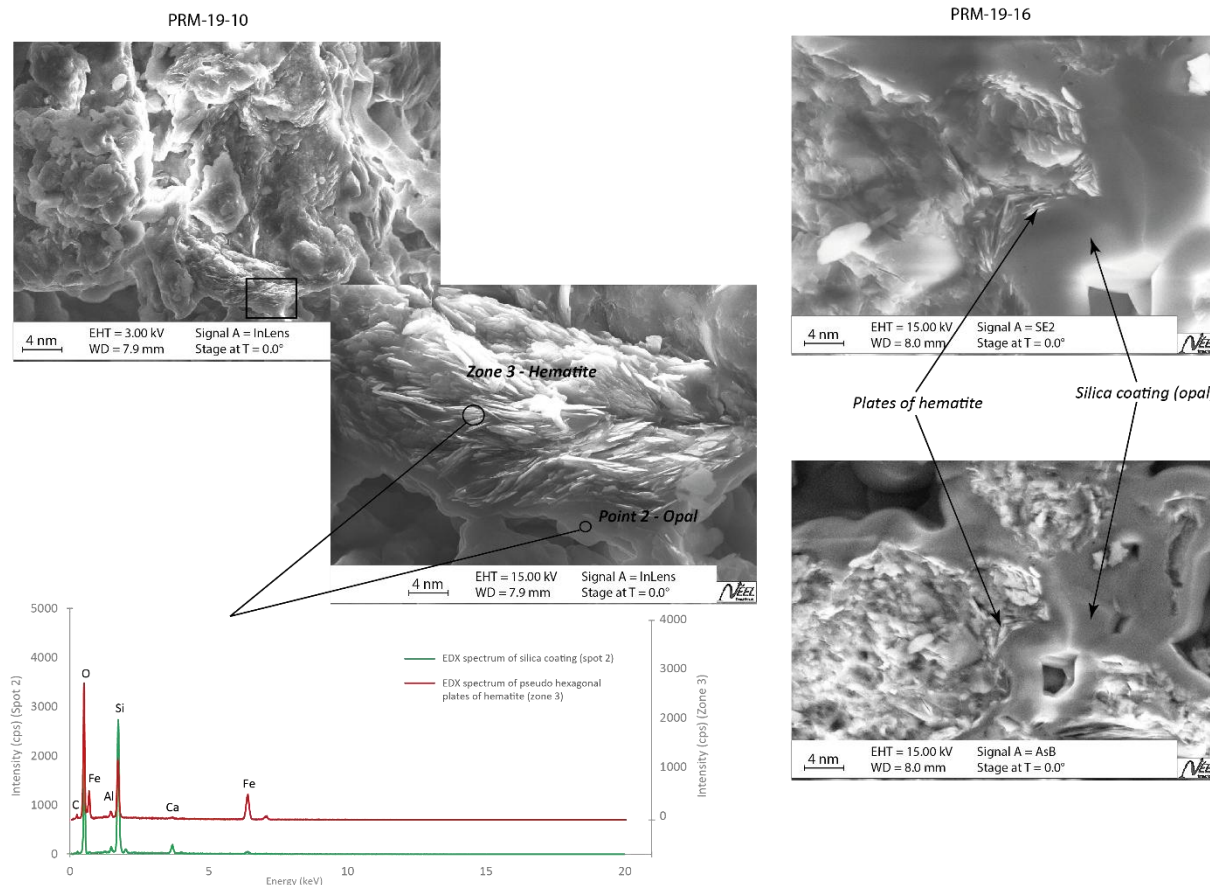
249

Figure 3: SEM observations of μ -S-ECA-05_prlvt_02. 1/ Hematite plate observation in Secondary Electron mode (SE); 2/ Pillow-like silica coating on surface in SE mode; White rectangle = Area of EDX spectra on the pillow-like silica coating.

250
 251 Concerning the μ -samples from the decorated walls, the same observations were noted, including
 252 pseudo-hexagonal platy hematite and strong indications of opal (S.I.1). Importantly, these samples
 253 showed significant opal development, with a complete coating of the pictorial matter to the extent that
 254 the morphology of the hematite was no longer observable on the surface (Figure 3). Weathered
 255 hematite plates seem to have been "ingested" by the silicate coating and could only be observed when
 256 a section was accessible on the surface of the sample (Figure 4 + S.I.2). However, preliminary studies

257 on the walls of Points Cave using portable spectroscopic techniques (pXRF and Raman) could not
258 identify the presence of opal coating *in situ* (Chanteraud *et al.*, 2020).

259



260

Figure 4: Hematite plates embedded in the silica coating on PRM-19-10 and PRM-19-16 μ -samples
(SEM observation in SE and BSE mode).

261

262

4.3 Opal identification by UV-fluorescence

263

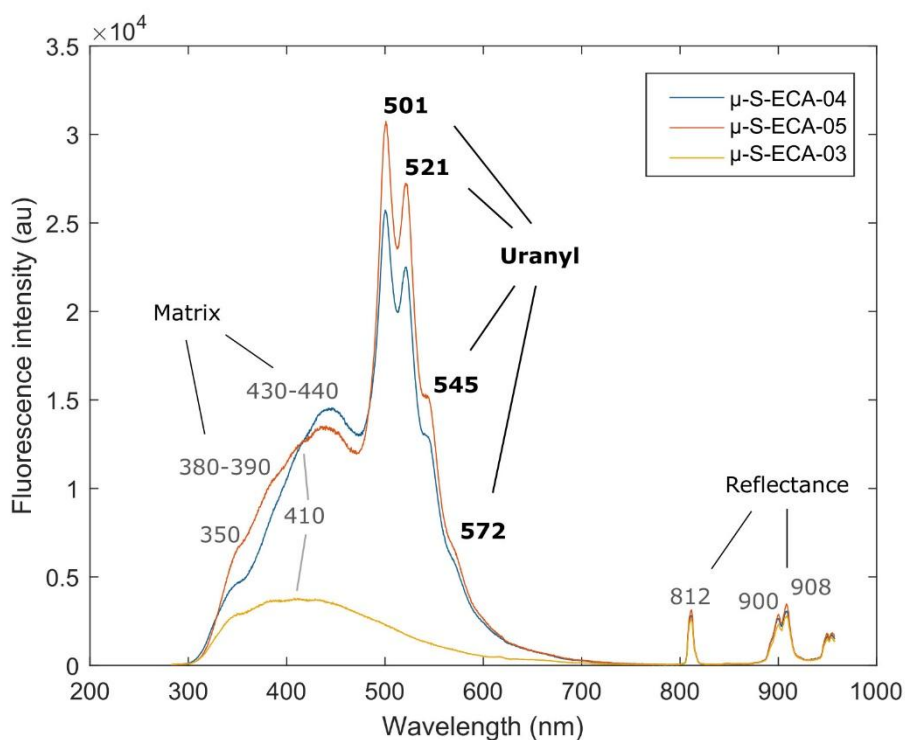
264 Fluorescence analyses were first performed on 3 flake μ -samples (μ S-ECA-03, μ S-ECA-04 and μ S-
265 ECA-05) that were previously characterized by different geochemical analyses and on which opal was
266 detected. Due to the small size of the samples (approximately 200 μ m), only a few localized spectra
267 were recorded. The spectra obtained could be divided into different emission regions depending on the
268 main signal sources (Figure 5, S.I.3):

269

270 - From 300 to 470 nm, this region corresponds to the fluorescence emission of the sample matrix.
271 Peaks and shoulders were detected at approximately 350 nm, 380-390 nm, 410 nm and 430-440
272 nm. According to the literature, they could be associated with organic matter entrapped in the
273 crystalline matrix (McGarry & Baker, 2000; Perrette *et al.*, 2000; Van Beynen *et al.*, 2001;
274 Perrette *et al.*, 2005; Quiers *et al.*, 2015) or with the silica material fluorescence response to
275 UV-light excitation (Boyko *et al.*, 2011; Garcia-Guinea *et al.*, 2013).

276

277 - From 470 to 750 nm, special features were identified in this part of the spectra for samples μ S-
278 ECA-04 and μ -S-ECA-05. They were characterized by a sequence of 3 defined peaks at 501,
279 521, and 545 nm and a shoulder at approximately 572 nm. These peaks were identical in all
280 spectra measured on μ -samples μ S-ECA-04 and μ -S-ECA-05 and coincided with the uranyl ion
281 spectrum in silica matrices based on a review in the literature (Table 3). Absence of uranyl
282 characteristic peaks on μ -S-ECA-03 can be attributed to the low opal occurrence on its surface
283 as observed with SEM.



284
 285 **Figure 5:** Mean fluorescence emission spectra (excitation: 266 nm) of samples μ -S-ECA-04, μ -S-
 286 ECA-05 and μ -S-ECA-03. Spectra are divided into three different regions as a function of the main
 287 fluorescence signal sources: sample matrix, uranyl ions and laser emission reflectance.

288
 289 Entrapment of uranyl ions in siliceous matrices, especially opal phases, is well documented in the
 290 literature (Zielinski, 1980; Kasdan *et al.*, 1981; Kinnunen & Ikonen, 1991; Neymark *et al.*, 2000;
 291 Fritsch *et al.*, 2001; Gaillou *et al.*, 2008; Devès *et al.*, 2012; Fritsch *et al.*, 2015; Othmane *et al.*, 2016).
 292 The strong affinity of uranyl groups for amorphous silica leads to a strong U-opal association, which is
 293 stable at the scale of geological time (Othmane *et al.*, 2016). As opal was the only silica phase
 294 identified on these samples, uranyl-specific spectra could be associated, in this case, with the presence
 295 of opal on samples, and UV fluorescence analysis represents an efficient tool for its identification.

296
 297 As opal detection was subject to uranyl fluorescence properties, detection using UV fluorescence was
 298 dependent on uranium entrapment in silica crystalline structures. In their study of opal gems from

299 different geographic and geological contexts, Gaillou *et al.* (2008) showed that not all opals are
 300 fluorescent. Opal fluorescence can be divided into two classes: blue fluorescence caused by intrinsic
 301 oxygen-related defects typical of amorphous silica structures and green fluorescence attributed to
 302 uranyl groups (Fritsch *et al.*, 2001, 2003), which is believed to be typical of common opals. A low
 303 content of U (≥ 1 ppm) automatically induces a green fluorescence response to UV light excitation.
 304 This content can reach more than 100 ppm in some deposits (Gaillou *et al.*, 2008). Garcia-Guinea *et*
 305 *al.* (2013) measured a uranium amount of 193 ppm in stalactites in Castanar Cave. Thus, detection of
 306 opal via UV fluorescence is not systematic but common, as a low content of uranium allows
 307 fluorescence emission. However, uranium concentration in Points Cave μ -samples have not been
 308 measured due to the particularly thin opal layer and the impossibility of destroying μ -samples.

309
310
311
312
313

314 **Table 3:** Fluorescence emission peaks for different opal or amorphous silica deposits reviewed in the
 315 *literature.*

	Fluorescence emission peaks (nm)				
Othmane <i>et al.</i> 2016	504	524	546	570	-
	504	523	545	573	-
Fritsch <i>et al.</i> 2015	504	524	546	572	604
Brennan & White 2013	502	520	-	-	-
Garcia-Guinea <i>et al.</i> 2013	505	524	543	569	-
<i>This study</i>	501	521	545	572	-

316
317

4.4 Opal visual detection under UV light

318

319 As explained previously, minerals containing uranyl ions (UO_2^{2+}) have been known to exhibit strong
320 fluorescence marked by specific spectral features and temporal characteristics since at least early 1900
321 (deNeufville *et al.*, 1981). The bright green fluorescence of uraniferous opal is a well-known
322 characteristic of this mineral phase and has been related to the presence of uranium (Gorobets *et al.*,
323 1977; Fritsch *et al.*, 2001). To evaluate whether this specificity can be used for opal detection, flake μ -
324 samples were exposed to UV light (see 3.1.1). The results show that μ -samples μ -S-ECA-04 and μ -S-
325 ECA-05 exhibited a bright green-light response (Figure 6). These two sample spectra contained
326 specific features corresponding to the fluorescence emission of uranyl ions. Green illumination was
327 thus associated with the presence of U-opal on these samples. The case of μ -sample μ -S-ECA-03 was
328 more complex. While the fluorescence spectrum did not show any spectral features associated with the
329 uranyl signal, localized greenish fluorescence could be distinguished on the sample. This could be
330 explained by a less precise measurement due to a more difficult targeting of opal because of the higher
331 sample size or more scattered opal distribution. Second, the sample surface was more coloured and
332 had more pictorial matter (cf. §4.1), suggesting decreased ability for detection.

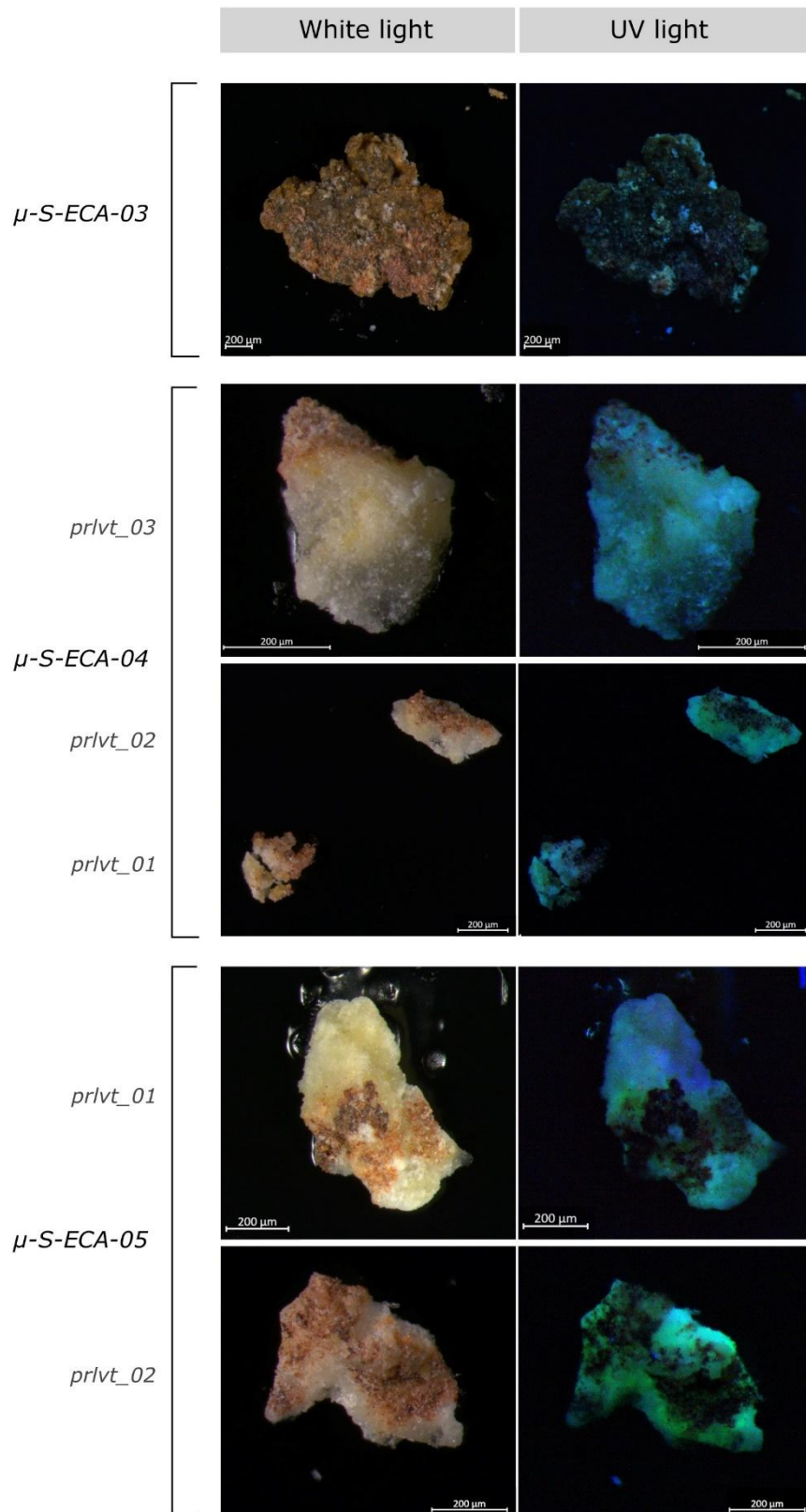


Figure 6: Photographs of μ -samples taken on flakes under white and UV light.

334

335

4.4 From the lab to the cave:

336

337

4.4.1 Comparison between UV methods

338

339 Considering that uranyl green illumination is representative of the presence of opal, detection
340 concordance between spectral and visual techniques was tested at a larger scale by comparing UV-
341 illuminated photographs with UV fluorescence cartography of flake S-ECA-05.

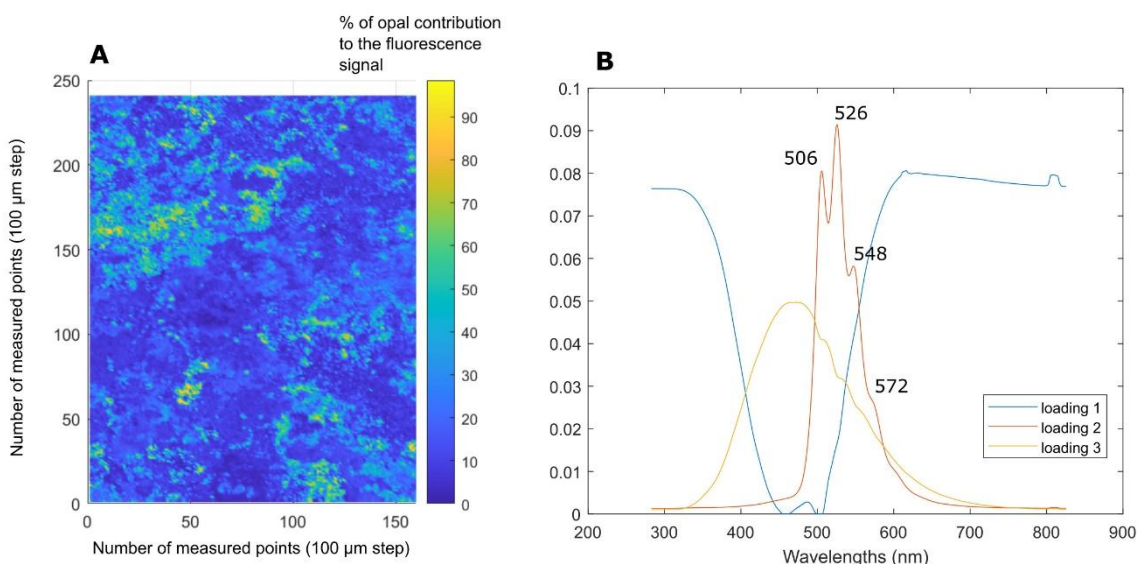
342

343 First, to evaluate UV LIF method accuracy at a larger scale, a second experiment was performed
344 directly on flake S-ECA-05. UV fluorescence cartography (100 x 100 μm resolution, S.I.4) showed a
345 range of spectra presenting uranyl spectral characteristics. Indeed, uranyl peaks present different
346 intensities or ratios compared to the fluorescence signal of the matrix, or can be not detected.
347 Assuming that the fluorescence signal can be interpreted as a mixing of a uranyl signal with a global
348 matrix signal, opal information was extracted from fluorescence cartography using a mixing
349 algorithm, MCR-ALS, with the MCR-ALS toolbox in MATLAB software (Jaumot *et al.*, 2015).
350 MCR-ALS has become a popular chemometric method in solving mixture analytical models. It is
351 based on an additive bilinear model of pure contributions that depends on the concentration and the
352 specific spectral sensitivity of each component. This algorithm can also be applied to obtain
353 quantitative information (Jaumot *et al.*, 2005; de Juan *et al.*, 2014; Zhang & Tauler, 2013).

354

355 A singular value decomposition (SVD) method was first applied on the entire raw dataset in the MCR
356 calculation to define the number of initial loadings (S.I.5). Based on the eigen values obtained with the
357 SVD method, three components were graphically determined as mainly contributors to the
358 fluorescence signal and represent 76.8% of the explained variance. These three initial loadings were
359 then calculated in the MCR-ALS method using the PURE algorithm, a commonly used method to find
360 the purest variable. MCR-ALS was then performed based on these 3 initial loadings on the same entire

361 dataset. Non-negativity constraint was applied for model optimization. For each spectrum, model
362 results ($r^2=99.8$) provided a proportion of each recalculated loading (Figure 7). The second loading
363 represents the uranyl spectrum from which is calculated a proportion of uranyl contribution to the total
364 fluorescence signal. This contribution can be associated with a proportion of opal at the sample surface
365 for each pixel as presented in Figure 7. The other loadings correspond to the contribution of different
366 fluorescence parts in the spectra related to the matrix fluorescence (loading 2) and to some specific
367 highly intense signals at the sample surface (loading 1), probably due to particular minerals.
368



369

Figure 7: MCR-ALS results: A/ Representation of the proportion of opal in the total fluorescence signal calculated from loading 2 on the S-ECA-05 surface, B/ Loadings obtained after model optimization.

370

371 Evaluation of opal proportions on the sample using this method is, however, subject to certain biases.
372 Similar to the majority of spectroscopic techniques, this detection method can only detect surface
373 deposits. Thus, opal mineralization located under other mineral or organic deposits cannot be detected.
374 Moreover, for quantitative measurement, the measurement sensitivity to changes in sample surface

375 microtopography must be taken into account. As the laser beam is focused on the surface, variations in
376 fluorescence intensities measured on the sample, and thus opal estimations, can be biased by
377 millimetric changes in surface relief.

378

379 This method remains effective in extracting information on opal mineralization even on heterogeneous
380 matrices, such as the Points Cave μ -samples. Due to its specific spectral shape, uranyl signal can be
381 easily extracted from mixed fluorescence signals. Mixing algorithms could provide quantitative
382 information if combined with calibration methods. Indeed, the MCR-ALS algorithm has been used for
383 the quantification of different target molecules based on various spectroscopic data (Mas *et al.*, 2010;
384 Araya *et al.*, 2017; Kumar *et al.*, 2018; Castro *et al.*, 2021). Regarding sample complexity, calibration
385 protocols based on standard references and prepared or artificial mixtures are difficult to apply (Araya
386 *et al.*, 2017). Quantification strategies need to be developed for archaeological materials, reaching a
387 balance between sample destruction and model result robustness, such as those developed for
388 hyperspectral data. Then, the estimated concentration accuracy will depend on the legitimacy of the
389 assumption made in the quantification strategy (Araya *et al.*, 2017).

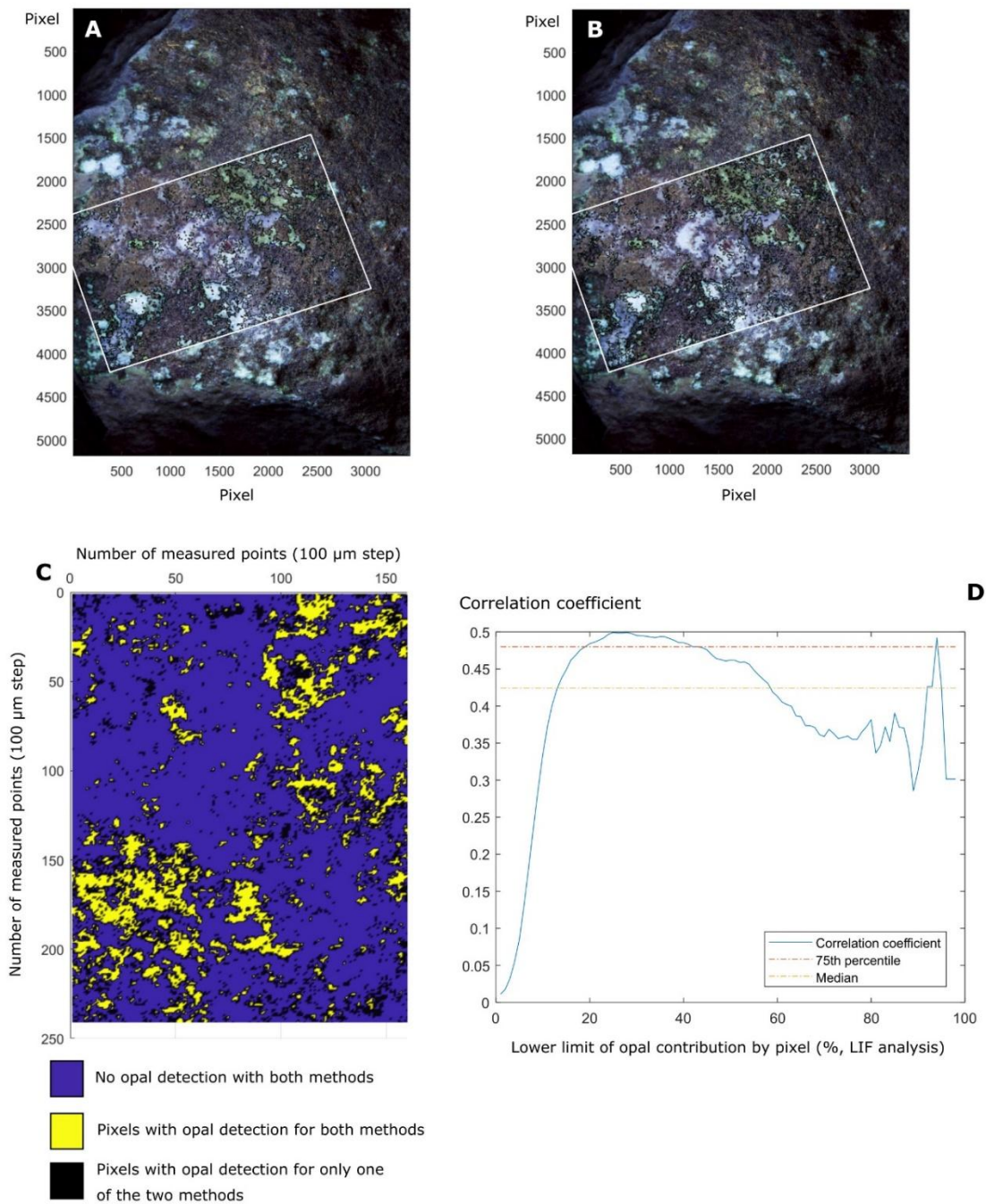
390

391 For field purpose, opal information provided by UV illumination and UV LIF methods were
392 compared. The green component of the RGB image was extracted from UV-light photos. The
393 grayscale image was subtracted to avoid the luminosity effect, and a threshold was applied to the
394 image obtained to select only pixels containing green colour (S.I.5). To help compare the opal
395 information provided by both techniques, images were aligned using point control selection and
396 geometric transformation functions in MATLAB.

397

398 The results show a high correspondence between spectral and visual detection methods (Figure 8). To
399 evaluate the efficiency of the optical method, opal cartographies with different detection limits were
400 simulated by modifying lower boundaries to select pixel associated with opal presence. These
401 boundaries are based on % of opal contribution to the fluorescence signal for spectroscopic

402 measurements. The best correlation coefficient ($R^2=0.50$) is obtained for an opal contribution
403 threshold of 25% of the total fluorescence signal. Graph D on figure 8 shows that optical method was
404 the most efficient when opal fluorescence emission contributed at least from 20% to 43% of the total
405 fluorescence signal of the sample. If the opal proportion limit for pixel selection is settled too low, the
406 number of pixels selected is too important to provide a good correlation and conversely. For example,
407 80% of pixels in the image were selected with a limit settled from 8% of opal contribution, providing a
408 correlation coefficient of only 0.24. The rather low correlation coefficient between both images could
409 mainly be explained by the point control selection and geometric transformation applied to readjust
410 them together. Angle disposition of the sample and detector combined with image resolution could
411 have led to difficulties in adjusting the images. Further research in the computational image domain
412 could improve the methodology and enhance the correlation between the two techniques.
413



414

Figure 8: Comparison of detection of opal mineralization on flake S-ECA-05 with UV illumination and UV LIF. A and B/ Photo under UV light and contour plot (black line) of opal presence calculated from the green component of the image (at least 8% of green) and from the MCR results (contribution of at least 25% of the total fluorescence) respectively for A and B, after geometric transformation (white square). C/ Cartography of pixels associated with the presence of opal comparing A and B (no

geometric transformation). D/ Correlation coefficient between opal presence images obtained with the two methods (% of opal contribution correspond to lower boundaries applied for pixels selection).

415

416 *4.4.2 Visual detection under UV light: field experiments*

417

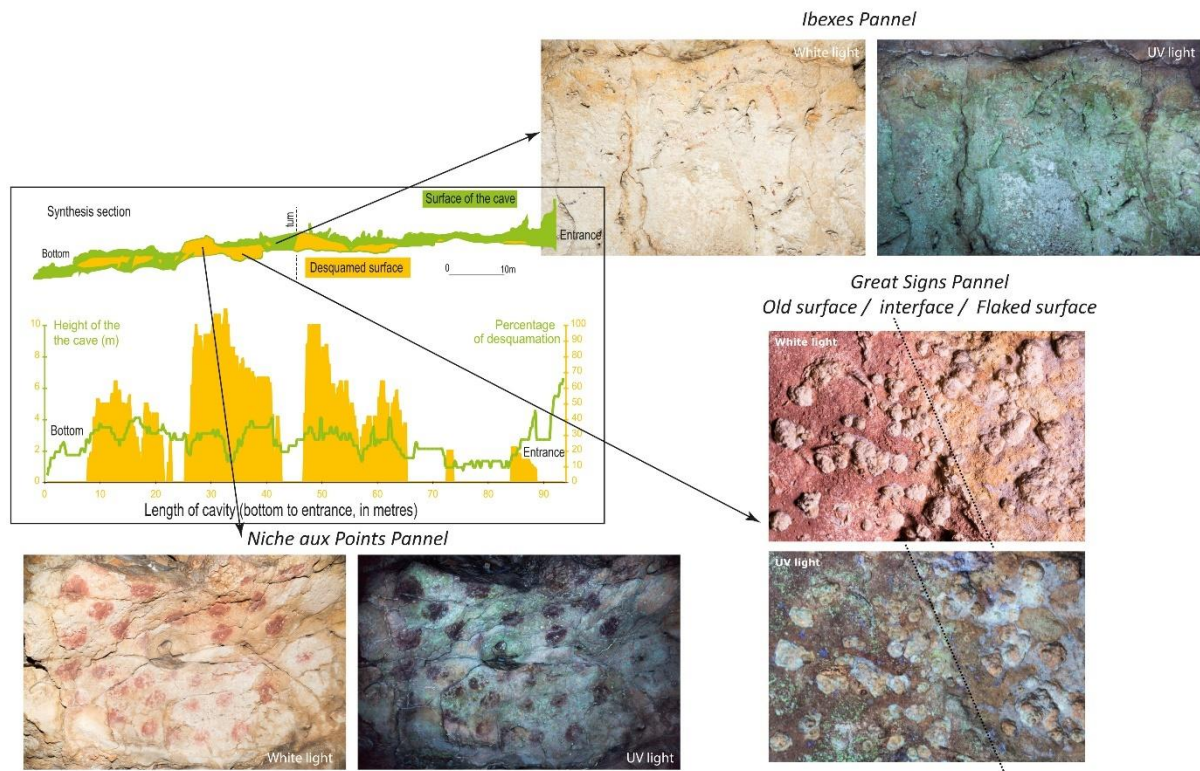
418 An *in situ* photographic protocol that alternated white light and UV illumination was applied to the
419 Points Cave walls. As shown in Figure 1, three rock art panels were investigated with one wall where
420 rock art was absent. Images were realized at both the wall and macroscopic scales.

421

422 At the wall scale, the rock art panels investigated (Niche aux Points, Bilobed Signs and Ibexes)
423 displayed large green fluorescent zones when illuminated by UV LEDs (Figure 9). This green
424 fluorescence response was consistent with preliminary results obtained in the laboratory on cave wall
425 flakes and μ -samples from these zones. Thus, UV illumination successfully enabled the detection of
426 opal coatings on these walls, according to the green response observed in photographs.

427

428 In contrast, no opal signal appeared clearly distinguishable in photographs of the wall situated a few
429 metres before the art panel (S.I.7). These photographs displayed greenish fluorescence mixed with
430 other signals, making it difficult to identify and extract green colour with accuracy. Spectroscopic
431 measurements need to be performed to precisely identify the presence of opal.



432

433 **Figure 9:** Topographic section of Points Cave with estimated flaking and location of white and UV

434 light photographs according to Jaillet & Monney, 2018.

435

436

437 Macroscopic-scale observations under UV light allowed the targeting of specific deposits or zones on
 438 cave walls. In the particular case of the Bilobed Signs panel, macroscopic investigation targeting
 439 flaking zones revealed a contrast between the rock art panel and the zones where flakes had detached
 440 from the wall. Indeed, the left part of the UV photograph (Figure 9) displayed numerous green
 441 fluorescent spots, whereas they were absent from the right part of the photograph. Efflorescence
 442 concretions on cave walls, which are widely spread in Points Cave, were also investigated, but the
 443 presence of opal has not yet been validated.

444

445

446

447

448 **5. Discussion: Implications of opal detection for rock art studies at Points Cave**

449

450 5.1 Contribution of UV fluorescence techniques

451

452 According to the first results obtained using the *in situ* UV illumination method and the preliminary
453 results obtained in the laboratory on cave wall flakes and μ -samples from rock art panels, *in situ*
454 measurements successfully detected the presence of opal in Points cave. Indeed, the green
455 fluorescence observed on Niche aux Points, Bilobed Signs and Ibexes panels suggests that opal
456 development covers a large area of cave walls, especially in rock art zones. Macroscopic observations
457 also help to provide initial insights into rock art-opal interactions, as UV light allows for the targeting
458 of specific deposits or zones on cave walls. It provides complementary information on opal
459 distribution and interaction with archaeological material. For example, investigation of the flaking
460 zone suggests a current absence of extended opal film or opal mineralization, probably due to
461 desquamation occurring on this wall.

462

463 However, the opal signal is not always clearly distinguishable, as observed on the wall outside of the
464 rock art zone or on coralloid concretions. Yet, these speleothems are known to contain a silica layer
465 enriched with uranium (Monney, 2019; Barbarand & Nouet, 2020). Alternating layers of silica and
466 calcite or the presence of calcite cover could explain the ambiguous signal. First, this highlights the
467 need for *in situ* fluorescence spectroscopic measurements to validate the photographic identification of
468 the opal mineral phase in cases where the green response is not clearly detectable. Second, colour
469 perception varies greatly from one image to another, even within the same site, making it difficult to
470 evaluate the mineral phase distribution. Even if camera and image treatment parameters influencing
471 colour display (white balance, exposure time, filters, etc.) can be easily standardized, lighting
472 variations (LED orientation, position, distance from wall, etc.) are difficult to homogenize. As this
473 paper presents preliminary results attempting to validate the detection method, no protocol for colour

474 calibration was applied. Further research on the Points Cave site will be subject to the development of
475 a colour calibration procedure.

476

477 Finally, UV illumination also highlights various types of deposits, sometimes not clearly detected
478 under white light. After fluorescence analyses in the laboratory or directly *in situ*, this technique could
479 help to detect other mineral or organic phases. Moreover, it is interesting to note that UV illumination
480 emphasizes the presence of pigments due to their iron composition. Indeed, iron ions are known to
481 have a quenching effect on the fluorescence signal, including that of uranyl ions (Backes, 2004;
482 Gaillou *et al.*, 2008; Chen *et al.*, 2011). Thus, pigments appear clearly as no fluorescence zones on UV
483 photographs, which can be an interesting tool for rock art analysis, such as determination of sampling
484 protocol or dermatoglyph analysis.

485

486 UV methodology appears to be an efficient non-invasive tool for the *in situ* identification of U-silica
487 mineralization, and of U-opal mineralization in this case. Due to the green fluorescence resulting from
488 UV excitation, it allows rapid *in situ* detection of the opal mineral phase with direct results and very
489 simple and low-cost equipment. As this method has already been applied with success in some caves,
490 rarely calcareous, for the detection of U-silica complex deposits or concretions, as in Castañar Cave
491 (Garcia-Guinea *et al.*, 2013), this study differs in two ways. First, to our knowledge, this method has
492 never been applied to opal detection in a rock art context. Second, we propose *in situ* opal
493 identification based on spectral features for result validation using a portable UV LIF instrument. This
494 instrument is currently in development and could not yet be taken into the cave, but preliminary tests
495 applied to flakes in the laboratory confirm its ability to detect opal. Finally, opal mineral
496 characterization can also be achieved with high-spatial resolution at the microscopic scale with a
497 laboratory UV LIF instrument. Spatially high-resolution fluorescence maps can also provide more
498 information on mineral phase repartition, development and interaction with other organic and mineral
499 phases present on the sample. Thus, the combination of these two methodologies provides a complete
500 solution for the identification and detection of opal mineralization in both sampling and analytical

501 strategies and *in situ* characterization.

502

503 5.2 What we know about Points Cave opal

504

505 The results obtained with the analyses presented in this paper and with UV methods applied to
506 samples and *in situ* have provided the first information on opal coatings in Points Cave. Indeed, based
507 on SEM analyses of flakes and μ -samples, Points Cave opal is associated with the amorphous opal
508 type (type A). XRD is usually performed for precise opal type determination (Curtis *et al.*, 2019).
509 However, in the case of Points Cave opal, this analysis is difficult to perform due to the opal thin layer
510 on calcareous substrate and iron-rich pigments. Analyses at macro- and microscopic scales suggest
511 thin film deposition as a mineralization type, such as silica skins observed at various rock art sites
512 (Watchman, 1990; Green *et al.*, 2017). This film appears to be deposited under or at the interface with
513 pigment and other crusts. SEM analyses show that the opal structure encapsulates hematite plates on
514 several samples, suggesting strong interactions with pictorial matter (Figure 4). Further studies must
515 be conducted to understand how these two phases interact, but a preliminary hypothesis regarding
516 dissolution and corrosion of hematite plaques by opal can be proposed.

517

518 The presence of uranyl ions entrapped in the opal structure was verified by UV spectroscopic analyses.
519 High fluorescence intensities of opal at Points Cave suggest significant content of uranium trapped in
520 the crystalline structure. Similar enrichment in uranium has been found in numerous common opals
521 (Amelin & Back, 2006). However, no quantification of uranium content has yet been realized.
522 Although uranium isotopic measurements were realized on speleothems from Points Cave (stalagmites
523 and coralloids), none was applied on flakes, or flake and wall μ -samples because of their destructive
524 character. According to the literature, as no minerals containing U^{4+} are known to fluoresce,
525 uraniferous silica precipitation involves oxidizing conditions sufficient to mobilize U^{6+} (Zielinski,
526 1982). For example, Garcia-Guinea *et al.* (2013) explained uranium-bearing opal deposition in
527 Castañar Cave by oxidation of host rocks with meteoritic waters. Zielinski (1982) explained that the

528 initial precipitation of silica was as an amorphous silica gel, with which dissolved uranium
529 coprecipitated before the silica gel dehydrated to form opal. The formation of uranyl-silica complexes
530 is favoured by the natural affinity between aqueous uranyl ions and the silica gel surface, which is
531 very sensitive to pH (optimum range = pH 5-5.5) (Garcia-Guinea *et al.*, 2013).

532

533 The *in situ* approach shows an important spread of this coating on Points Cave walls, especially on
534 rock art panels. Concerning the walls a few metres before the rock art panels, the presence of opal
535 needs to be confirmed by spectroscopic measurement and laboratory analyses. Points Cave chronology
536 is constrained by different periods marked by cave wall evolution under climatic and anthropogenic
537 factors (Monney & Jaillet, 2019). The presence of opal mineralization throughout its formation and
538 developmental processes could provide insights into cave chronology. A flaking period was identified
539 subsequent to ornamentation, resulting from mechanical expansion or desquamation, affecting the
540 deepest zones of the cave, and possibly concurrent with gelifraction during MIS2 (Marine Isotope
541 Stage 2) (Monney & Jaillet, 2019). As described previously, UV photographs indicated the absence of
542 a well-developed opal film in the flaking zone, suggesting that opal formation occurred principally
543 before this flaking period. This could also explain why photographs taken on walls between the cave
544 angle and the rock art sectors displayed less marked fluorescence, as this zone presents high flaking
545 rates (Jaillet & Monney, 2018) (Figure 9).

546

547 The chronology of opal deposits over art paintings and drawings cannot be confirmed at this stage.
548 SEM observations show that opal mineralization colonizes empty spaces under, below, and inside
549 pictorial matter. These observations suggest opal postdeposition over painting realization, although
550 prior mineralization cannot be ruled out.

551

552 Thus, ongoing studies are crucial in completing opal coating characterization in Points Cave. This is a
553 tool in understanding cave wall and pigment interactions throughout the factors and processes of opal
554 formation and other mineralization.

555

556 *5.3 Opal factors and formation*

557

558 Mineralization origin and formation mechanisms and factors are clues for understanding past climate
559 and cave wall evolution. As this paper presents preliminary results, only hypotheses for opal origin
560 and formation are presented.

561

562 Opal, as a hydrated mineral, is associated with fluid circulation. Thus, water is generally involved in
563 precipitation, and silica has to be in solution before precipitation (Chauviré *et al.*, 2017). In Points
564 Cave, the presence of silica coating with high uranium content in the limestone context supports the
565 hypothesis of mineralization originating from groundwater. Wall humidification and water
566 physicochemical properties directly influence the coating formation rate. In very wet sites, the silica
567 skin growth rate can reach 0.25 mm per millennia, whereas occasionally wet sites present a
568 mineralization rate on the order of 0.02 mm per millennia (Aubert *et al.*, 2004). Silica coatings can
569 only be formed and preserved if low infiltration volumes occur, as higher volumes favour dissolution
570 of soluble compounds and decrease silica precipitation (Aubert *et al.*, 2004).

571

572 Chauviré *et al.* (2017) explained that even though opal is found in various geological contexts, three
573 main types of formation can be identified: 1) hydrothermal activity, 2) biological precipitation and 3)
574 continental weathering. As no hydrothermal activity was identified at Points Cave, only the latter two
575 types can be involved in opal formation at this site.

576

577 Biological formation of opal in caves is less documented than hydrothermal alteration and continental
578 weathering. Various microbial forms and algae have been observed to be associated with opal in
579 caves, such as siliceous algal diatoms (Northup *et al.*, 2001), and are often linked to coralloid
580 concretions. In the case of Points Cave, a few microscopic and cave wall μ -sample observations show
581 undetermined structures containing high carbon content, which could be associated with biological

582 activity. Nevertheless, the hypothesis of biological formation of opal cannot be ruled out or confirmed
583 at this stage.

584

585 Continental weathering is defined by rock transformation by meteoric water and a precipitation
586 temperature below 50°C, in contrast to hydrothermal alteration (Chauviré *et al.*, 2017). Silica anions
587 released by this process precipitate because of fluid supersaturation due to various changes in
588 conditions, such as pH or temperature (Devès *et al.*, 2012; Chauviré *et al.*, 2017). Thus,
589 supersaturation of silica solutions may be initiated by a drop in temperature or pH, or an increase in
590 salinity. When a solution is supersaturated in SiO₂, silicic acid could polymerize to form a colloidal
591 suspension from which amorphous silica can precipitate. Polymerization is controlled by temperature
592 (decreasing T° increases the polymerization rate), degree of supersaturation, salinity and mainly pH
593 (maximum polymerization rate around pH 7.5; minimum polymerization rate under pH 3 and above 9)
594 (Devès *et al.*, 2012). One of the most efficient pH-driven mechanisms for silica precipitation involves
595 acidification of highly alkaline solutions (Zielinski, 1982). Such alkaline conditions are not common,
596 but in the case of calcite-dominant material in sediment, pH could reach this threshold (Karkanis *et*
597 *al.*, 1999). Freezing temperature has also been shown to help supersaturation, polymerization and
598 rapid precipitation of opal, whereas low or moderate temperatures induce slow polymerization
599 (months or years) (Devès *et al.*, 2012). Cryo-segregation is another reported genesis, caused by
600 moisture freezing on cave walls, which concentrates dissolved salts. They precipitate out in the case of
601 supersaturation of the solution (Devès *et al.*, 2012). As opal formation probably occurred between the
602 Upper Palaeolithic and the Last Glacial Maximum and because freezing temperatures have been
603 shown to have modified Points Cave wall topography, a temperature decrease represents a realistic
604 factor for opal formation. However, there is currently a lack of evidence to confirm this hypothesis.

605

606 To help understand opal formation, the source of silica and uranium forming this mineralisation can
607 also be questioned. Silica can originate from 1) superficial cover, 2) host rock, or 3) volcanic ash in a
608 continental weathering context (Devès *et al.*, 2012). Volcanic ash is an interesting hypothesis, as it is

609 assumed to provide both high contents of silica and uranium, and because the Ardèche region had
610 recent volcanic episodes during the Upper Palaeolithic. Indeed, Nomade *et al.* (2016) dated volcanic
611 eruptions in the Bas-Vivarais region between 29 ± 10 ka and 35 ± 8 ka and suggested that Chauvet
612 rock art, 35 km away, could depict volcanic eruption representations. The current alluvial plain and the
613 lowest former alluvial level (+8 m) deposits contain much basaltic material partly derived from Bas-
614 Vivarais lava, which were subjected to intense erosion and weathering in the alluvium terraces
615 (Genuite *et al.*, 2021). Thus, the location and chronology of the volcanic activity (approximately 45
616 km from Points Cave) represent an interesting origin hypothesis for both silica and uranium contents
617 in opal. However, determining the origin of uranyl-enriched silica solutions is difficult with our
618 current information. Another hypothesis for silica solution origin can be supported by the presence of
619 a marl layer within the Urgonian limestone, which constitutes the cave environment (Sadier, 2013); or
620 by pebbles originating from the Ardèche River and providing silica by infiltration from the overlaying
621 alluvium terrace or by river deposition (Mocochain *et al.*, 2009; Genuite *et al.*, 2021).

622
623 Thus, understanding the origin and mineralization factors that influence opal formation could provide
624 information on chemical and physical processes occurring on the cave wall surface. According to
625 Green *et al.* (2017), this knowledge is “crucial for targeted sample collection and the application of a
626 range of dating techniques as well as for the development of conservation strategies”.

627

628 *5.4 Chronology and dating*

629

630 Red pigments used in rock art are difficult to date precisely (Aubert *et al.*, 2007). Thus, several studies
631 have proposed indirect dating methods using associated mineral deposits interlaying pictorial matter to
632 date or to provide chronological constraints on rock paintings (Watchman, 1990; Aubert *et al.*, 2007;
633 Aubert *et al.*, 2017), such as opal coatings.

634

635 Indeed, in the first place, opal coating could help to precise relative chronology thanks to knowledge

636 regarding climatic and environmental factors controlling its mineralization, and to its distribution on
637 walls in comparison to other deposits and archaeological material.

638
639 Amorphous silica skins have been used for radiocarbon analyses based on organic remains trapped by
640 mineralization, such as diatoms or algal matter, on different Australian rock art sites (Watchman,
641 2000; Morwood *et al.*, 2010). However, as silica coatings may contain various organic materials, each
642 presenting a specific radiocarbon signature, dating could result in a mixture of different ages by
643 incorporation of younger or older material (Aubert *et al.*, 2017; Green *et al.*, 2017). In addition, the
644 formation processes of these coatings are not fully understood, requiring great caution when using
645 radiocarbon methods (Aubert *et al.*, 2017). Using compound-specific carbon analyses could
646 potentially avoid this problem (Aubert *et al.*, 2017) but are more difficult to apply to thin deposits,
647 especially in rock art contexts.

648
649 Moreover, opal often contains high uranium contents, which could be used for high-precision dating
650 with methods such as $^{230}\text{U}/\text{Th}$ or U/Pb (Zielinski, 1980; Oster *et al.*, 2017). Because of opal's ability to
651 concentrate uranium from water while rejecting Pb and Th, amorphous silica is an interesting
652 alternative to carbonate minerals (Amelin & Back, 2006). Indeed, $^{230}\text{Th}/\text{U}$ and U/Pb methods have
653 been applied to opal and have provided reliable ages (Neymark & Paces, 2013). They enable
654 chronological constraints or dating hydrogenic subsurface water flow, pedogenesis, and processes
655 such as ore formation deposits (Neymark & Paces, 2013). They also have been applied in the case of
656 paleoclimate reconstruction in silica speleothem studies (Lundberg *et al.*, 2010). Depending on the
657 formation processes, opal coating could thus be used for dating purposes.

658
659 In rock art research, dating of amorphous silica deposits could be used as an age constraint for rock
660 drawing events, depending on the pigments and mineral phase superposition. In their study, Aubert *et*
661 *al.* (2007) performed U-series dating on a 2.5 mm thick calcite coating using the MC-ICPMS
662 technique, allowing high spatial and temporal resolution. Even though only micrograms of samples are

663 needed, authors (Aubert *et al.*, 2007; Aubert *et al.*, 2017) have suggested that for samples with U
664 concentrations > 1 ppm, sampling could be largely reduced, and LIBS techniques could also be
665 applied *in situ* with a 100-200 µm diameter ablation spot. As opal concentrates more U than calcite,
666 these techniques appear to be possible. However, for some authors, the application of uranium series
667 dating to silica skins appears difficult to achieve (Green *et al.*, 2017). Sampling that provides sufficient
668 intact fragments for LA-ICP-MS analysis without damaging rock paintings is one of the main issues
669 regarding this application. The difficulty of performing closed system conditions and replicability tests
670 for evaluating dating reliability has also been highlighted by authors.

671
672 Moreover, methods for opal detection could offer supplemental help before sampling for dating.
673 Indeed, precise targeting of uranium-bearing opal enables identification of pure silica phases in mixed
674 samples, detection of high uranium contents or impurity avoidance. In the case of thin layer deposits,
675 such as in coralloids, sampling could decrease dating accuracy when mixing different layers (Devès *et*
676 *al.*, 2012). Tracking the location of opal phases could avoid this issue by spatially constraining
677 sampling.

678 679 *5.5 Implication of opal mineral characterization for conservation of rock art material*

680
681 Taphonomy represents a range of transformations affecting archaeological material that distort
682 archaeological records. Thus, rock paintings have undergone a plurality of transformations impacting
683 pigment longevity, colour and identification (Bednarik, 1994; Huntley, 2012; Chalmin *et al.*, 2018;
684 Rousaki *et al.*, 2018; Defrasne *et al.*, 2019). The exceptional of Points Cave dermatoglyphs has no
685 comparison with other associated parietal sites in Ardèche and begs the question of opal impact on
686 pigment conservation.

687
688 If pigment weathering can be influenced by their own properties by inducing changes in surface area,
689 albedo, light transmissivity or moisture (Huntley, 2012), mineral deposits have been recognized to be

690 important factors in rock art taphonomy (Chalmin *et al.*, 2018). In addition to analytical impacts,
691 knowledge of mineral phases is essential because it informs us regarding the physical and chemical
692 impacts on pictorial matter and whether they favour conservation or degradation effects. Mineral
693 phase characterization is thus an important part of conservation strategies, and adapted identification
694 and analytical methods are needed.

695
696 The association of silica skins composed of opal and pigments has been frequently observed at rock art
697 sites, mainly in open-air sites on sandstone and quartzite substrates in Australia or Canada (Watchman,
698 1990; Aubert *et al.*, 2004; Aubert *et al.*, 2012; Huntley, 2012). Some studies have suggested that
699 pigment binding in silica coatings aids rock art visual preservation (Watchman, 1990), providing a
700 resistant layer to chemical weathering. SEM observations on Points Cave flake and wall μ -samples
701 indeed suggest a strong interaction between pigments and opal, as mineralization penetrates pigment
702 deposits. If the quality of Points Cave paintings tends to corroborate this hypothesis, exfoliation
703 impacting silica skins observed at some sites should also be mentioned, as it could cause removal of
704 associated pigments (Aubert *et al.*, 2004; Green *et al.*, 2017). Thus, exploiting the observed benefits of
705 silica film deposits for conservation strategies has not yet been proven (Green *et al.*, 2017).
706 Furthermore, it has also been observed at open-air sites that silica skins could reduce the colour tone of
707 paintings and drawings at some locations (Green *et al.*, 2017).

708

709 **6. Conclusion**

710

711 The methodological development proposed in this paper was motivated by the identification of opal in
712 different contexts: *in situ*, in the laboratory, on centimetric objects and on μ -samples. The aim of this
713 identification is to question the possibility of accessing the specificities of the colouring matter applied
714 on the walls (petrography and geochemistry). Therefore, *in situ* identification of silica coating
715 observed in the laboratory was crucial for further studies on pigment characterization.

716

717 The results obtained on flakes and flake μ -samples from Points Cave show that UV LIF is an efficient
718 technique to detect and identify uranyl-silica complexes, even on heterogeneous and complex surfaces.
719 Although opal coating detection is limited by the outcropping nature of the deposit, UV LIF
720 spectroscopy offers a rapid and non-invasive tool that can easily be brought to the site and positioned
721 in front of the decorated panels. A photograph of green bright fluorescence emitted by opal was used
722 here as a method for *in situ* detection of this mineral coating. A comparison with the UV LIF method
723 shows a great correspondence between the two methods. The first tests of UV illumination in the cave
724 highlight the need to develop an accurate measurement protocol, especially to homogenize light and
725 colour, and the need to validate the identification using UV LIF spectroscopy. In addition to further
726 methodological development, UV optical technique shows great potential because it successfully
727 detects the presence of opal and its distribution on rock art panels.

728

729 The results obtained with our methodology provide insights into disturbances in the classical *in situ*
730 spectroscopic analyses (pXRF) observed at Points Cave (Chanteraud *et al.*, 2021). The identification
731 and characterization of opal coating is thus essential because its impact on *in situ* analysis could
732 disturb the detection of iron-oxide spectroscopic signal in case of Raman analysis for example. For
733 this reason, we propose early, on-site observations combined with sampling of surrounding material,
734 such as fallen flakes from cave walls, as an alternative strategy to i) characterize pigment-associated
735 mineral phases, ii) choose the best site-adapted combination of techniques and devices for *in situ*
736 analyses and iii) define laboratory analytical strategies depending on the pictorial matter environment.
737 Moreover, optical methods with *in situ* visual detection, such as the UV light illumination method
738 proposed in this paper, represent an interesting tool to add to sampling and analytical strategies.
739 Visualization at a larger scale of the presence and distribution of mineral deposits that could interfere
740 with pigment analyses is a great help in locating sampling or *in situ* measurements to avoid
741 interference.

742

743 In addition to analytical impacts, the detection and identification of mineral phases can provide
744 valuable information on the pigment environment and human practice chronology. If speleothems are
745 considered an accurate archive for past climate and environment, other mineral deposits could provide
746 informative records on the setting and evolution of archaeological evidence. Applying a specific
747 methodology for their characterization is thus an efficient tool in improving rock art knowledge.

748

749 Thanks to opal mineralization detection utilizing UV methodologies on cave walls, a discussion on its
750 formation and associated factors, such as climatic, hydrologic or geomorphologic conditions over time
751 can be started. Thus, the mineral form described as opal can provide elements on cave natural history.

752

753 **Acknowledgements**

754

755 We would like to thank Frédérique Charlot, microscopist at CMTC (INPE, Grenoble).
756 Funding was provided by ANR LabCom SpecSolE, DRAC Occitanie, DRAC AURA
757 (Pigmentoθήque project), French Ministry of Culture and University Savoie Mont Blanc.

758

759 **Conflict of interest disclosure**

760 The authors declare they have no conflict of interest relating to the content of this article.

761

762 **Data, script and code availability**

763 *S.I.1. Macroscopic pictures and SEM datas of flakes μ -samples:*

764 <https://doi.org/10.6084/m9.figshare.16832593.v2>

765 <https://doi.org/10.6084/m9.figshare.16832557.v3>

766 <https://doi.org/10.6084/m9.figshare.16832452>

767 <https://doi.org/10.6084/m9.figshare.16832605>

768

769 *S.I.2. Macroscopic pictures and SEM datas of rock art μ -samples:*

770 <https://doi.org/10.6084/m9.figshare.19142243.v1>

771 <https://doi.org/10.6084/m9.figshare.19142267.v1>

772 <https://doi.org/10.6084/m9.figshare.19142276.v1>

773 <https://doi.org/10.6084/m9.figshare.19142300.v1>

774 <https://doi.org/10.6084/m9.figshare.19142351.v1>

775 <https://doi.org/10.6084/m9.figshare.19142354.v1>

776 <https://doi.org/10.6084/m9.figshare.19142366.v1>

777 <https://doi.org/10.6084/m9.figshare.19142372.v1>

778 <https://doi.org/10.6084/m9.figshare.19142375.v1>

779 <https://doi.org/10.6084/m9.figshare.19142381.v1>

780 <https://doi.org/10.6084/m9.figshare.19142384.v1>

781 <https://doi.org/10.6084/m9.figshare.19142387.v1>

782

783 *S.I.3. Single UV fluorescence measurement (raw data):*

784 <https://doi.org/10.6084/m9.figshare.16837180.v1>

785

786 *S.I.4. UV fluorescence cartography measurement (raw data):*

787 <https://doi.org/10.6084/m9.figshare.16837324.v3>

788

789 *S.I.5. UV fluorescence data processing (Matlab script):*

790 <https://doi.org/10.6084/m9.figshare.16837405.v2>

791

792 *S.I.6. pXRF result of in situ analysis at the Points Cave:*

793 <https://doi.org/10.6084/m9.figshare.9791405.v1>

794 <https://doi.org/10.6084/m9.figshare.9791210.v1>

795

796 *S.I.7. In situ UV photographs*

797 <https://doi.org/10.6084/m9.figshare.19316588.v1>

798

799 **Bibliography**

800 Amelin, Y., Back, M., 2006. Opal as a U–Pb geochronometer: search for a standard. *Chemical*

801 *Geology* 232, 67–86. <https://doi.org/10.1016/j.chemgeo.2006.02.018>

802

803 Araya, J.A., Carneiro, R.L., Arévalo, C., Freer, J., Castillo, R. del P., 2017. Single pixel quantification

804 strategies using middle infrared hyperspectral imaging of lignocellulosic fibers and MCR-ALS

805 analysis. *Microchemical Journal* 134, 164–172. <https://doi.org/10.1016/j.microc.2017.05.019>

806

807 Aubert, M., 2012. A review of rock art dating in the Kimberley, Western Australia. *Journal of*

808 *Archaeological Science* 39, 573–577. <https://doi.org/10.1016/j.jas.2011.11.009>

809

810 Aubert, M., Watchman, A., Arsenault, D., Gagnon, L., 2004. L'archéologie rupestre du Bouclier

811 canadien : Potentiel archéométrique. *Canadian Journal of Archaeology/Journal Canadien*

812 *d'Archéologie* 51–74. <http://www.jstor.org/stable/41103470>

813

814 Aubert, M., O'Connor, S., McCulloch, M., Mortimer, G., Watchman, A., Richer-LaFlèche, M., 2007.

815 Uranium-series dating rock art in East Timor. *Journal of Archaeological Science* 34, 991–996.

816 <https://doi.org/10.1016/j.jas.2006.09.017>

817

818 Aubert, M., Brumm, A., Taçon, P.S., 2017. The timing and nature of human colonization of Southeast

819 Asia in the late Pleistocene: A rock art perspective. *Current Anthropology* 58, S553–S566.

820 <https://doi.org/10.1086/694414>

821

822 Backes, C. J., 2004. More Than Meets the Eye: Fluorescence Photography for Enhanced Analysis of
823 Pictographs. *Journal of California and Great Basin Anthropology*, 24(2), 193–206.

824 <http://www.jstor.org/stable/27825774>

825

826 Barbarand, J., Nouet, J., 2020. Pétrographie et minéralogie des coralloïdes de la grotte au Points, in:
827 Monney J. (Dir.). *Projet Datation Grottes Ornées : Rapport d'activité 2020. Grotte Aux Points*
828 (Aiguèze). Rapport Non Publié., Ministère de La Culture, SRA Occitanie, Montpellier.

829

830 Bassel, L., 2017. Genèse de faciès calcitiques : mondmilch et coralloïdes. Étude multiphysique des
831 concrétions de la grotte laboratoire de Leye (Dordogne) (Thèse). Université Bordeaux Montaigne.

832 <https://tel.archives-ouvertes.fr/tel-01729035>

833

834 Bednarik, R.G., 1994. A taphonomy of palaeoart. *Antiquity* 68, 68–74.

835 <https://doi.org/10.1017/S0003598X00046202>

836

837 Boyko, V., Dovbeshko, G., Fesenko, O., Gorelik, V., Moiseyenko, V., Romanyuk, V., others, 2011.
838 New optical properties of synthetic opals infiltrated by DNA. *Molecular Crystals and Liquid Crystals*
839 535 (1), 30-41. <https://doi.org/10.1080/15421406.2011.537888>

840

841 Brennan, E. S., White, W. B., 2013. Luminescence of speleothems: a comparison of sources and
842 environments. *Journal of Cave & Karst Studies*, 75(3).

843

844 Castro, R.C., Ribeiro, D.S., Santos, J.L., Páscoa, R.N., 2021. Near infrared spectroscopy coupled to
845 MCR-ALS for the identification and quantification of saffron adulterants: Application to complex
846 mixtures. *Food Control* 123, 107776. <https://doi.org/10.1016/j.foodcont.2020.107776>

847

848 Chalmin, E., Hoerlé, S.H., Reiche, I., 2018. Taphonomy on the Surface of the Rock Wall: Rock-Paint-
849 Atmosphere Interactions. Bruno David; Ian J. McNiven. The Oxford Handbook of the Archaeology
850 and Anthropology of Rock Art, Oxford Handbook. <https://hal.archives-ouvertes.fr/hal-01801656/>

851

852 Chalmin, E., Salomon, H., Chassin de Kergommeaux, A., Chanteraud, C., 2019. Construction d'une
853 Pigmentoθήque : un outil pour comprendre l'approvisionnement en matériaux colorants durant la
854 Préhistoire. : Rapport d'activité 2019. [Rapport de recherche] DRAC/SRA; Auvergne Rhône Alpes.
855 2019. [hal-02429867](https://hal.archives-ouvertes.fr/hal-02429867)

856

857 Chanteraud, C., 2020. Matières colorantes et grottes ornées des gorges de l'Ardèche. Méthodes
858 d'analyse des ressources et liens culturels au Paléolithique supérieur : application à la grotte aux Points
859 (Aiguèze, Gard, France) (Thèse). Université Savoie Mont Blanc. [https://tel.archives-ouvertes.fr/tel-](https://tel.archives-ouvertes.fr/tel-03184877)
860 [03184877](https://tel.archives-ouvertes.fr/tel-03184877)

861

862 Chanteraud, C., Chalmin, E., Hoerlé, S., Salomon, H., Monney, J., 2019. Relation entre les matières
863 colorantes issues des fouilles et des parois ornées. Méthodologie et première perspective comparative
864 à la Grotte aux Points (Aiguèze, Gard, France). *Karstologia* pp 1-12. [https://hal.archives-](https://hal.archives-ouvertes.fr/hal-01756858/)
865 [ouvertes.fr/hal-01756858/](https://hal.archives-ouvertes.fr/hal-01756858/)

866

867 Chanteraud, C, Chalmin, É., Lebon, M., Salomon, H., Jacq, K., Noûs, C., Delannoy, J.-J., Monney, J.
868 2021. Contribution and limits of portable X-ray fluorescence for studying Palaeolithic rock art: a case
869 study at the Points cave (Aiguèze, Gard, France). *Journal of Archaeological Science: Reports* 37:
870 102898. <https://doi.org/10.1016/j.jasrep.2021.102898>

871

872 Chauviré, B., Rondeau, B., Mangold, N., 2017. Near infrared signature of opal and chalcedony as a
873 proxy for their structure and formation conditions. *European Journal of Mineralogy* 29, 409–421.

874 <https://doi.org/10.1127/ejm/2017/0029-2614>

875

876 Chen, C.-C., Pestov, D., Nelson, J.D., Anderson J.E. and G. Tepper, 2011. Uranyl Soil Extraction and
877 Fluorescence Enhancement by Nanoporous Silica Gel: pH effects. *J Fluoresc* 21, 119–124.

878 <https://doi.org/10.1007/s10895-010-0695-0>

879

880 Curtis, N.J., Gascooke, J.R., Johnston, M.R., Pring, A., 2019. A review of the classification of opal
881 with reference to recent new localities. *Minerals* 9, 299. <https://doi.org/10.3390/min9050299>

882

883 De Juan, A., Jaumot, J., Tauler, R., 2014. Multivariate Curve Resolution (MCR). Solving the mixture
884 analysis problem. *Analytical Methods* 6, 4964–4976. <https://doi.org/10.1039/C4AY00571F>

885

886 Defrasne, C., Chalmin, E., Bellot-Gurlet, L., Thirault, E., and G. André, 2019. From archeological
887 layers to schematic rock art? Integrated study of the Neolithic pigments and pigmented rocks at the
888 Rocher du Château (Western Alps, Savoie, France). *Archaeol Anthropol Sci* 11, 6065–6091.

889 <https://doi.org/10.1007/s12520-019-00882-9>

890

891 Delvigne, Jean E. 1998. *Atlas of Micromorphology of Mineral Alteration and Weathering*. The
892 Canadian Mineralogist 3. Ottawa: Paris: Mineralogical Association of Canada; ORSTOM.

893

894 DeNeufville, J., Kasdan, A., Chimenti, R., 1981. Selective detection of uranium by laser-induced
895 fluorescence: a potential remote-sensing technique. 1: Optical characteristics of uranyl geologic
896 targets. *Applied Optics* 20, 1279–1296. <https://doi.org/10.1364/AO.20.001279>

897

898 Deschamps, E.B., Chauvet, J.M., Hillaire, C., 2018. La grotte aux Points d'Aiguèze : récits de

899 découverte d'une ornementation pariétale. *Karstologia* 72, 13–14.

900

901 Devès, G., Perroux, A.-S., Bacquart, T., Plaisir, C., Rose, J., Jaillet, S., Ghaleb, B., Ortega, R., Maire,
902 R., 2012. Chemical element imaging for speleothem geochemistry: Application to a uranium-bearing
903 corallite with aragonite diagenesis to opal (Eastern Siberia, Russia). *Chemical Geology* 294, 190–202.
904 <https://doi.org/10.1016/j.chemgeo.2011.12.003>

905

906 Flörke, O., Graetsch, H., Röller, K., Martin, B., Wirth, R., 1991. Nomenclature of micro-and non-
907 crystalline silica minerals. *Neues Jahrbuch für Mineralogie, Abhandlungen* 163, 19–42.

908

909 Fritsch, E., Mihut, L., Baibarac, M., Baltog, I., Ostrooumov, M., Lefrant, S., Wery, J., 2001.
910 Luminescence of oxidized porous silicon: Surface-induced emissions from disordered silica micro-to
911 nanotextures. *Journal of Applied Physics* 90, 4777–4782. <https://doi.org/10.1063/1.1410887>

912

913 Fritsch, E., Wéry, J., Jonusauskas, G., Faulques, E., 2003. Transient photoluminescence from highly
914 disordered silica-rich natural phases with and without nanostructures. *Physics and chemistry of*
915 *minerals* 30, 393–400. <https://doi.org/10.1007/s00269-003-0329-z>

916

917 Fritsch, E., Megaw, P.K., Spano, T.L., Chauviré, B., Rondeau, B., Gray, M., Hainschwang, T., Renfro,
918 N., 2015. Green-luminescing hyalite opal from Zacatecas, Mexico. *J. Gemmol* 34, 490–508.

919

920 Gaillou, E., Delaunay, A., Rondeau, B., Bouhnik-le-Coz, M., Fritsch, E., Cornen, G., Monnier, C.,
921 2008. The geochemistry of gem opals as evidence of their origin. *Ore Geology Reviews* 34, 113–126.
922 <https://doi.org/10.1016/j.oregeorev.2007.07.004>

923

924 Garcia-Guinea, J., Fernandez-Cortes, A., Alvarez-Gallego, M., García-Antón, E., Casas-Ruiz, M.,
925 Blázquez-Pérez, D., Teijón, O., Cuezva, S., Correcher, V., Sanchez-Moral, S., 2013. Leaching of

926 uranyl–silica complexes from the host metapelite rock favoring high radon activity of subsoil air: case
927 of Castañar cave (Spain). *Journal of Radioanalytical and Nuclear Chemistry* 298, 1567–1585.

928 <https://doi.org/10.1007/s10967-013-2587-7>

929

930 Genuite, K., Delannoy, JJ., Bahain, JJ., Gresse M., Jaillet S., Philippe A., Pons-Branchu E., Revil A.,
931 and P. Voinchet, 2021. Dating the landscape evolution around the Chauvet-Pont d'Arc cave. *Sci*

932 *Rep* 11, 8944. <https://doi.org/10.1038/s41598-021-88240-5>

933

934 Gorobets, B., Engoyan, S., Sidorenko, G., 1977. Investigation of uranium and uranium-containing
935 minerals by their luminescence spectra. *Soviet Atomic Energy* 42, 196–202.

936 <https://doi.org/10.1007/BF01121388>

937

938 Green, H., Gleadow, A., Finch, D., Hergt, J., Ouzman, S., 2017. Mineral deposition systems at rock art
939 sites, Kimberley, Northern Australia—Field observations. *Journal of Archaeological Science: Reports*

940 14, 340–352. <https://doi.org/10.1016/j.jasrep.2017.06.009>

941

942 Huntley, J., 2012. Taphonomy or paint recipe: In situ portable x-ray fluorescence analysis of two
943 anthropomorphic motifs from the Woronora Plateau, New South Wales. *Australian Archaeology* 75,

944 78–94. <https://doi.org/10.1080/03122417.2012.11681952>

945

946 Huntley, J., Aubert, M., Ross, J., Brand, H. E., Morwood, M. J., 2015. One colour, (at least) two
947 minerals: a study of mulberry rock art pigment and a mulberry pigment ‘quarry’ from the Kimberley,

948 northern Australia. *Archaeometry* 57 (1), 77–99. <https://doi.org/10.1111/arcm.12073>

949

950 Jaillet, S., Monney, J., 2018. Analyse 3D des volumes et remplissages souterrains de la grotte aux
951 Points au temps des fréquentations paléolithiques (Aiguèze, Gard). *Karstologia* 72, 27–36.
952 <https://hal.archives-ouvertes.fr/hal-01878453/>
953
954 Jaumot, J., Gargallo, R., de Juan, A., Tauler, R., 2005. A graphical user-friendly interface for MCR-
955 ALS: a new tool for multivariate curve resolution in MATLAB. *Chemometrics and intelligent*
956 *laboratory systems* 76, 101–110. <https://doi.org/10.1016/j.chemolab.2004.12.007>
957
958 Jaumot, J., de Juan, A., Tauler, R., 2015. MCR-ALS GUI 2.0: New features and applications.
959 *Chemometrics and Intelligent Laboratory Systems* 140, 1–12.
960 <https://doi.org/10.1016/j.chemolab.2014.10.003>
961
962 Karkanias, P., Kyparissi-Apostolika, N., Bar-Yosef, O., Weiner, S., 1999. Mineral assemblages in
963 Theopetra, Greece: a framework for understanding diagenesis in a prehistoric cave. *Journal of*
964 *Archaeological Science* 26, 1171–1180. <https://doi.org/10.1006/jasc.1998.0354>
965
966 Kasdan, A., Chimenti, R.J.L., deNeufville, J.P., 1981. Selective detection of uranium by laser-induced
967 fluorescence: a potential remote-sensing technique. 2: Experimental assessment of the remote sensing
968 of uranyl geologic targets. *Appl. Opt.* 20, 1297–1307. <https://doi.org/10.1364/AO.20.001297>
969
970 Kinnunen, K.A., Ikonen, L., 1991. Opal, a new hydromorphic precipitate type from gravel deposits in
971 southern Finland. *Bulletin of the Geological Society of Finland* 63, 95–104.
972
973 Kumar, K., 2018. Application of Genetic Algorithm (GA) Assisted Partial Least Square (PLS)
974 Analysis on Trilinear and Non-trilinear Fluorescence Data Sets to Quantify the Fluorophores in

975 Multifluorophoric Mixtures: Improving Quantification Accuracy of Fluorimetric Estimations of Dilute
976 Aqueous Mixtures. *Journal of fluorescence* 28, 589–596. <https://doi.org/10.1007/s10895-018-2221-8>
977

978 Lundberg, J., Brewer-Carias, C., and D., McFarlane, 2010. Preliminary results from U-Th dating of
979 glacial-interglacial deposition cycles in a silica speleothem from Venezuela. *Quaternary Research*, 74
980 (1), 113-120. <https://doi.org/10.1016/j.yqres.2010.03.005>
981

982 Mas, S., de Juan, A., Tauler, R., Olivieri, A.C., Escandar, G.M., 2010. Application of chemometric
983 methods to environmental analysis of organic pollutants: a review. *Talanta* 80, 1052–1067.
984 <https://doi.org/10.1016/j.talanta.2009.09.044>
985

986 Mauran, G., Lebon, M., Détroit, F., Caron, B., Nankela, A., Pleurdeau, D., Bahain, J.-J. 2019. First in
987 Situ PXRF Analyses of Rock Paintings in Erongo, Namibia: Results, Current Limits, and Prospects.
988 *Archaeological and Anthropological Sciences* 11 (8): 4123–45. [https://doi.org/10.1007/s12520-019-](https://doi.org/10.1007/s12520-019-00787-7)
989 [00787-7](https://doi.org/10.1007/s12520-019-00787-7)
990

991 McGarry, S. F., Baker, A., 2000. Organic acid fluorescence: applications to speleothem
992 palaeoenvironmental reconstruction. *Quaternary Science Reviews* 19(11), 1087-1101.
993 [https://doi.org/10.1016/S0277-3791\(99\)00087-6](https://doi.org/10.1016/S0277-3791(99)00087-6)
994

995 Mocochain L., Audra, P., Clauzon, G., Bellier, O., Bigot, J.-Y., Parize, O., and P. Monteil, 2021. The
996 effect of river dynamics induced by the Messinian Salinity Crisis on karst landscape and caves:
997 Example of the Lower Ardèche river (mid Rhône valley), *Geomorphology*, 106 (1–2), 46-61.
998 <https://doi.org/10.1016/j.geomorph.2008.09.021>.
999

1000 Monger, H.C., Kelly, E.F., 2002. Silica minerals. *Soil mineralogy with environmental applications* 7,
1001 611–636.

1002

1003 Monney, J., 2011. Projet Datation Grottes Ornées : Rapport d'activité 2011. Grotte aux Points
1004 (Aiguèze). Rapport non publié, Ministère de la Culture, SRA Occitanie, Montpellier.

1005

1006 Monney, J., 2018. L'art pariétal paléolithique de la grotte aux Points d'Aiguèze: définition d'un
1007 dispositif pariétal singulier et discussion de ses implications. *Karstologia* 72, 45–60.

1008

1009 Monney, J. 2019. Projet Datation Grottes Ornées : Rapport 2019 (12ème volet) : 12.1. Grotte aux
1010 Points (Aiguèze). [Rapport de recherche] Ministère de la Culture, SRA Occitanie, Montpellier. 2019.
1011 [hal-01972949](https://hal.archives-ouvertes.fr/hal-01972949)

1012

1013 Monney, J., Jaillet, S., 2019. Phases de fréquentations humaines, ornementation pariétale et processus
1014 naturels : Mise en place d'un cadre chronologique pour la grotte aux Points d'Aiguèze. *Karstologia* 72,
1015 49–62. <https://hal.archives-ouvertes.fr/hal-01957634/>

1016

1017 Morwood, M.J., Walsh, G.L., Watchman, A.L., 2010. AMS radiocarbon ages for beeswax and
1018 charcoal pigments in north Kimberley rock art. *Rock Art Research: The Journal of the Australian*
1019 *Rock Art Research Association (AURA)* 27 (1), 3–8.
1020 <https://search.informit.org/doi/10.3316/informit.153070840500133>

1021

1022 Neymark, L., Paces, J.B., 2013. Ion-probe U–Pb dating of authigenic and detrital opal from Neogene-
1023 Quaternary alluvium. *Earth and Planetary Science Letters* 361, 98–109.
1024 <https://doi.org/10.1016/j.epsl.2012.11.037>

1025

1026 Neymark, L.A., Amelin, Y.V., Paces, J.B., 2000. 206Pb–230Th–234U–238U and 207Pb–235U
1027 geochronology of Quaternary opal, Yucca Mountain, Nevada. *Geochimica et Cosmochimica Acta* 64,
1028 2913–2928. [https://doi.org/10.1016/S0016-7037\(00\)00408-7](https://doi.org/10.1016/S0016-7037(00)00408-7)

1029

1030 Nomade, S., Genty, D., Sasco, R., Scao, V., Féruglio, V., Baffier, D., Guillou, H., Bourdier, C.,
1031 Valladas, H., Reigner, E., others, 2016. A 36,000-year-old volcanic eruption depicted in the Chauvet-
1032 Pont d' Arc Cave (Ardèche, France)? PloS one 11(1), e0146621.
1033 <https://doi.org/10.1371/journal.pone.0146621>

1034

1035 Northup, K.H., Diana, Lavoie, 2001. Geomicrobiology of caves: a review. Geomicrobiology journal
1036 18, 199–222. <https://doi.org/10.1080/01490450152467750>

1037

1038 Oster, J.L., Kitajima, K., Valley, J.W., Rogers, B., Maher, K., 2017. An evaluation of paired $\delta^{18}\text{O}$ and
1039 $(^{234}\text{U}/^{238}\text{U})_0$ in opal as a tool for paleoclimate reconstruction in semi-arid environments. Chemical
1040 Geology 449, 236–252. <https://doi.org/10.1016/j.chemgeo.2016.12.009>

1041

1042 Othmane, G., Allard, T., Vercouter, T., Morin, G., Fayek, M., Calas, G., 2016. Luminescence of
1043 uranium-bearing opals: Origin and use as a pH record. Chemical Geology 423, 1–6.
1044 <https://doi.org/10.1016/j.chemgeo.2015.12.010>

1045

1046 Perrette, Y., Delannoy, J.-J., Bolvin, H., Cordonnier, M., Destombes, J.-L., Zhilinskaya, E.A.,
1047 Aboukais, A., 2000. Comparative study of a stalagmite sample by stratigraphy, laser induced
1048 fluorescence spectroscopy, EPR spectrometry and reflectance imaging. Chemical Geology 162, 221–
1049 243. [https://doi.org/10.1016/S0009-2541\(99\)00069-8](https://doi.org/10.1016/S0009-2541(99)00069-8)

1050

1051 Perrette, Y., Delannoy, J. J., Desmet, M., Lignier, V., Destombes, J. L., 2005. Speleothem organic
1052 matter content imaging. The use of a Fluorescence Index to characterise the maximum emission

1053 wavelength. *Chemical Geology* 214 (3-4), 193-208. <https://doi.org/10.1016/j.chemgeo.2004.09.002>
1054

1055 Pons-Branchu, E., Bourrillon, R., Conkey, M.W., Fontugne, M., Fritz, C., Gárate, D., Quiles, A.,
1056 Rivero, O., Sauvet, G., Tosello, G., 2014. Uranium-series dating of carbonate formations overlying
1057 Paleolithic art: interest and limitations. *Bulletin de la Société préhistorique française* 211–224.
1058 <http://www.jstor.org/stable/24364541>
1059

1060 Quiers, M., Perrette, Y., Chalmin, E., Fanget, B., Poulénard, J., 2015. Geochemical mapping of
1061 organic carbon in stalagmites using liquid-phase and solid-phase fluorescence. *Chemical Geology* 411,
1062 240-247. <https://doi.org/10.1016/j.chemgeo.2015.07.012>
1063

1064 Quiles, A., Fritz, C., Alcaide, M.Á.M., Pons-Branchu, E., Torti, J.L.S., Tosello, G., Valladas, H.,
1065 2015. Chronologies croisées (C-14 et U/Th) pour l'étude de l'art préhistorique dans la grotte de Nerja:
1066 méthodologie. Presented at the *Sobre rocas y huesos: las sociedades prehistóricas y sus*
1067 *manifestaciones plásticas*, UCO Press. Editorial de la Universidad de Córdoba, pp. 420–427.
1068

1069 Rousaki, A., Vargas, E., Vázquez, C., Aldazábal, V., Bellelli, C., Calatayud, M. C., Hajduk A.,
1070 Palacios O., Moens L., and P. Vandenabeele, 2018. On-field Raman spectroscopy of Patagonian
1071 prehistoric rock art: Pigments, alteration products and substrata. *TrAC Trends in Analytical*
1072 *Chemistry*, 105, 338-351. <https://doi.org/10.1016/j.trac.2018.05.011>
1073

1074 Sadier, B., 2013. 3D et géomorphologie karstique : La grotte Chauvet et les cavités des Gorges de
1075 l'Ardèche (Thèse). Université de Savoie, Le-Bourget-Du-Lac. <https://hal.univ-smb.fr/tel-01070711/>
1076

1077 Salomon, Hélène, Claire Chanteraud, Aurélie Chassin de Kergommeaux, Julien Monney, Jean-Victor
1078 Pradeau, Éric Goemaere, Yvan Coquinot, and Emilie Chalmin. 2021. 'A Geological Collection and

1079 Methodology for Tracing the Provenance of Palaeolithic Colouring Materials'. *Journal of Lithic*
1080 *Studies* 8 (1): 38-p. <https://doi.org/10.2218/jls.5540>
1081
1082 Savitzky, A., Golay, M.J.E., 1964. Smoothing and Differentiation of Data by Simplified Least Squares
1083 Procedures. *Analytical Chemistry*. 36, 1627–1639. <https://doi.org/10.1021/ac60214a047>
1084
1085 Shao, Q.-F., Pons-Branchu, E., Zhu, Q.-P., Wang, W., Valladas, H., Fontugne, M., 2017. High
1086 precision U/Th dating of the rock paintings at Mt. Huashan, Guangxi, southern China. *Quaternary*
1087 *Research* 88, 1–13. <https://doi.org/10.1017/qua.2017.24>
1088
1089 Trosseau, Antoine, Anne Maigret, Yvan Coquinot, and Ina Reiche, 2021. In Situ XRF Study of Black
1090 Colouring Matter of the Palaeolithic Figures in the Font-de-Gaume Cave. *Journal of Analytical Atomic*
1091 *Spectrometry* 36 (11): 2449–59. <https://doi.org/10.1039/D1JA00202C>
1092
1093 Valladas, H., Pons-Branchu, E., Dumoulin, J.P., Quiles, A., Sanchidrián, J.L., Medina-Alcaide, M.Á.,
1094 2017. U/Th and ¹⁴C Crossdating of Parietal Calcite Deposits: Application to Nerja Cave (Andalusia,
1095 Spain) and Future Perspectives. *Radiocarbon* 59, 1955–1967. <https://doi.org/10.1017/RDC.2017.120>
1096
1097 Van Beynen, P., Bourbonniere, R., Ford, D., Schwarcz, H., 2001. Causes of colour and fluorescence in
1098 speleothems. *Chemical Geology* 175 (3-4), 319-341. [https://doi.org/10.1016/S0009-2541\(00\)00343-0](https://doi.org/10.1016/S0009-2541(00)00343-0)
1099
1100 Vignaud, C., Salomon, H., Chalmin, E., Geneste, J.-M., Menu, M. 2006. Le groupe des « bisons
1101 adossés » de Lascaux. Étude de la technique de l'artiste par analyse des pigments. *L'Anthropologie*
1102 110 (4): 482–99. <https://doi.org/10.1016/j.anthro.2006.07.008>.
1103
1104 Watchman, A., 1990. What are silica skins and how are they important in rock art conservation?
1105 *Australian Aboriginal Studies* 1, 21–29.

1106 <https://search.informit.org/doi/10.3316/ielapa.154935712026809>

1107

1108 Watchman, A., 2000. A review of the history of dating rock varnishes. *Earth-Science Reviews* 49,

1109 261–277. [https://doi.org/10.1016/S0012-8252\(99\)00059-8](https://doi.org/10.1016/S0012-8252(99)00059-8)

1110

1111 Zhang, X., Tauler, R., 2013. Application of multivariate curve resolution alternating least squares

1112 (MCR-ALS) to remote sensing hyperspectral imaging. *Analytica chimica acta* 762, 25–38.

1113 <https://doi.org/10.1016/j.aca.2012.11.043>

1114

1115 Zielinski, R.A., 1980. Uranium in secondary silica; a possible exploration guide. *Economic Geology*

1116 75, 592–602. <https://doi.org/10.2113/gsecongeo.75.4.592>

1117

1118 Zielinski, R.A., 1982. Uraniferous opal, Virgin Valley, Nevada: Conditions of formation and

1119 implications for uranium exploration. *Journal of Geochemical Exploration* 16, 197–216.

1120 [https://doi.org/10.1016/0375-6742\(82\)90010-3](https://doi.org/10.1016/0375-6742(82)90010-3)

1121